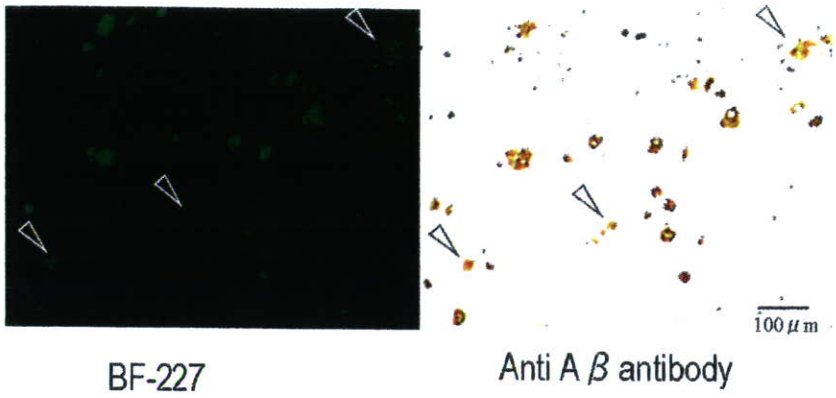

Figure 3. Neuropathological staining of amyloid plaques with BF-227 in AD brain sections. Sps and diffuse plaques (arrow head) were clearly stained with BF-227.

mice. In a subacute study, intravenous administration of BF-227 in tested doses did not produce any significant changes in general behavior and body weight. After 14 days post-treatment period, the mice did not show any microscopic alteration on pathological examination.

Other actions of BF-227

In the autoradiographic image using [^{11}C]BF-227, a specific binding pattern in the AD brain section was observed in the grey matter including SPs.

In the brain sections of PS1/APP Tg mice after intravenous injection of BF-227, numerous fluorescent spots were observed in the neocortex and hippocampus of the brain. These fluorescent spots corresponded to those of Aβ immunostaining in the same section.

Discussion and future prospects

BF-227 has high binding affinity to Aβ fibrils, remarkable stainability for SPs, high permeability of BBB, and fast clearance from normal brain tissue. The toxicity study of BF-227 indicates the sufficient safety margin of this compound for PET probe. Currently, we have investigated the clinical trial of [^{11}C]BF-227 in healthy subjects and in AD patients. This trial will elucidate the binding characteristics *in vivo* and the clinical usefulness of the probe in humans, and the results will be published by this summer or autumn.

Recently, we have introduced three novel compounds as candidate probes for *in vivo* imaging of tau pathology in the AD brain; 4-[2-(2-benzoimidazolyl) ethenyl]-N, N-diethylbenzenamine (BF-126), 2-[(4-methylamino) phenyl] quinoline (BF-158), and 2-(4-aminophenyl) quinoline (BF-170) (14) (Figure 4). In neuropathological examination,

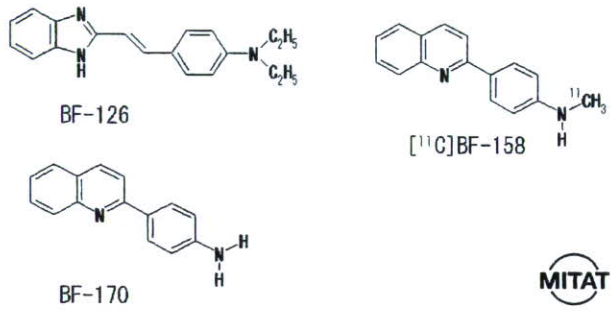

Figure 4. Chemical structures of our tau specific probes.

BF-126, BF-158, and BF-170 clearly stained NFTs, neuropil threads, and paired helical filament-type neuritis in the AD brain section. In addition, NFTs was labeled by 11C-labeled BF-158 with autoradiography. These findings suggest the potential usefulness of quinoline and benzimidazole derivatives for *in vivo* imaging of tau pathology in AD.

Several 11-C labeled probes for detecting SPs in AD patients have been reported from some teams. The short half-life (20 min) of 11-C, however, may limit the usefulness of these probes for a widespread application. Comparable 18-F labeled probes may supplant the clinical need due to the longer half-life of the isotope (109.7 min) (15). Further studies to develop 18-F labeled PET probes for the imaging of SPs are currently under way in some teams, including ours.

Unlike Alois Alzheimer, we now have access to instrumentation that allows visualization of the human brain *in vivo*. Brain imaging has become a part of the routine clinical assessment of dementia disorder (16). Recently, anti-amyloid agents such as Aβ vaccine and selective secretase inhibitors have been developed for the causal therapy of AD patients. AD patients all over the world may be

effectively diagnosed and treated by a combination of presymptomatic diagnosis and causal therapy.

Acknowledgement

The author thanks all the present and past members of our team and collaborators.

This study was financially supported by the Special Coordination Funds for Promoting Science and Technology, the Health and Labour Sciences Research Grants for Translational research from Ministry of Health, Labour and Welfare, Japan, the Program for Promotion of Fundamental Studies in Health Science of the National Institute of Biomedical Innovation, the New Energy and Industrial Technology Development Organization (NEDO), the Novartis foundation for Gerontological Research, the AstraZeneca Research Grant, and the Mitsui Sumitomo Insurance Welfare.

References

1. Shoji M, Golde TE, Ghiso J, Cheung TT, et al. Production of the Alzheimer amyloid beta protein by normal proteolytic processing. Science. 1992;258:126–9.
2. Lee VM, Balin BJ, Otvos L, Jr. Trojanowski JQ. A68: a major subunit of paired helical filaments and derivatized forms of normal Tau. Science. 1991;251:675–8.
3. Nordberg A. PET imaging of amyloid in Alzheimer's disease. Lancet Neurol. 2004;3:519–27.
4. Klunk WE, Debnath ML, Pettegrew JW. Chrysamine-G binding to Alzheimer and control brain: autopsy study of a new amyloid probe. Neurobiol Aging. 1995;16:541–8.
5. Skovronsky DM, Zhang B, Kung MP, Kung HF, et al. In vivo detection of amyloid plaques in a mouse model of Alzheimer's disease. Proc Natl Acad Sci U S A. 2000;97:7609–14.
6. Klunk WE, Bacskai BJ, Mathis CA, Kajdasz ST, et al. Imaging Abeta plaques in living transgenic mice with multi-photon microscopy and methoxy-X04, a systemically administered Congo red derivative. J Neuropathol Exp Neurol. 2002;61:797–805.
7. Shoghi-Jadid K, Small GW, Agdeppa ED, Kepe V, et al. Localization of neurofibrillary tangles and beta-amyloid plaques in the brains of living patients with Alzheimer disease. Am J Geriatr Psychiatry. 2002;10:24–35.
8. Klunk WE, Engler H, Nordberg A, Wang Y, et al. Imaging brain amyloid in Alzheimer's disease with Pittsburgh Compound-B. Ann Neurol. 2004;55:306–19.
9. Verhoeff NP, Wilson AA, Takeshita S, Trop L, et al. In-vivo imaging of Alzheimer disease beta-amyloid with [11C]SB-13 PET. Am J Geriatr Psychiatry. 2004;12:584–95.
10. Bacskai BJ, Klunk WE, Mathis CA, Hyman BT. Imaging amyloid-beta deposits in vivo. J Cereb Blood Flow Metab. 2002;22:1035–41.
11. Okamura N, Suemoto T, Shiomitsu T, Suzuki M, et al. A novel imaging probe for in vivo detection of neuritic and diffuse amyloid plaques in the brain. J Mol Neurosci. 2004;24:247–55.
12. Okamura N, Suemoto T, Shimadzu H, Suzuki M, et al. Styrylbenzoxazole derivatives for in vivo imaging of amyloid plaques in the brain. J Neurosci. 2004;24:2535–41.
13. Shimadzu H, Suemoto T, Suzuki M, Shiomitsu T, et al. Novel probes for imaging amyloid-beta: F-18 and C-11 labeling of 2-(4-aminostyryl)benzoxazole derivatives. Journal of Labelled Compounds & Radiopharmaceuticals. 2004;47:181–90.
14. Okamura N, Suemoto T, Furumoto S, Suzuki M, et al. Quinoline and benzimidazole derivatives: candidate probes for in vivo imaging of tau pathology in Alzheimer's disease. J Neurosci. 2005;25:10857–62.
15. Chandra R, Kung MP, Kung HF. Design, synthesis, and structure-activity relationship of novel thiophene derivatives for beta-amyloid plaque imaging. Bioorg Med Chem Lett. 2006;16:1350–2.
16. Nordberg A. Is amyloid plaque imaging the key to monitoring brain pathology of Alzheimer's disease in vivo? Eur J Nucl Med Mol Imaging. 2004;31:1540–3.

Imaging Amyloid Pathology in the Living Brain

Nobuyuki Okamura[a,*], Shozo Furumoto[b], Hiroyuki Arai[c], Ren Iwata[d], Kazuhiko Yanai[a] and Yukitsuka Kudo[b]

[a]*Department of Pharmacology, Tohoku University School of Medicine, Sendai 980-8575, Japan,* [b]*Tohoku University Biomedical Engineering Research Organization (TUBERO), Sendai 980-8575, Japan,* [c]*Center for Asian Traditional Medicine, Department of Geriatrics and Gerontology, Tohoku University School of Medicine, Sendai 980-8574, Japan,* [d]*Division of Radiopharmaceutical Chemistry, Cyclotron and Radioisotope Center, Tohoku University, Sendai 980-8578, Japan*

Abstract: Progressive deposition of amyloid plaques in the brain, which begins before the appearance of cognitive decline, is an initiating event in the pathogenesis of Alzheimer's disease. Therefore, noninvasive detection of amyloid pathology is important for presymptomatic diagnosis and preventive therapy for Alzheimer's disease. Recent research advances have enabled the *in vivo* imaging of amyloid pathology in humans using nuclear medicine technology. Several amyloid-binding agents have been developed and evaluated by positron emission tomography (PET) and single photon emission computed tomography (SPECT) for their use as contrast agents. Available clinical evidence indicates that amyloid imaging enables the early diagnosis of Alzheimer's disease with high accuracy and suggests its usefulness for the prediction of progression to Alzheimer's disease in subjects with mild cognitive impairment and probably also in cognitively normal individuals. Another application of this technology is as a surrogate marker for monitoring brain amyloid. In this review, we describe recent progress in the development of amyloid imaging technology and human clinical trials.

Keywords: Amyloid, Alzheimer's disease, Positron emission tomography (PET), molecular imaging, senile plaque, neurofibrillary tangle.

INTRODUCTION

Alzheimer's disease (AD) is the most common cause of dementia in the elderly. The definitive diagnosis of AD relies on postmortem assessment, with characteristic pathological changes such as neuron death, senile plaques (SPs), and neurofibrillary tangles (NFTs). Currently, the amyloid cascade hypothesis is widely accepted to account for the pathogenesis of AD [1]. SP is mainly composed of amyloid β (Aβ), which is generated by proteolytic reaction of β and γ-secretase from the amyloid precursor protein (APP). In this hypothesis, the mismetabolism of APP is the initiating event in AD pathogenesis. Excessive generation of Aβ causes aggregation of Aβ and the formation of SPs, and this is followed by the formation of NFTs, neuron death, neurotransmitter deficit, and cognitive decline. If this hypothesis is correct, optimal therapeutic strategies for interrupting the disease process should be directed toward modifying the generation, clearance, and cytotoxicity of Aβ.

Early diagnosis and treatment of AD is important in maintaining the patient's activities of daily living as long as possible and preventing the patient from becoming bedridden. A notable feature of AD is a discrepancy between clinical symptoms and pathological findings in the brain (Fig. (1)). Even in the clinically early stage of dementia, a large amount of SP is already present in the brain [2, 3]. These changes in the brain probably start 10–20 years before clinical symptoms appear. Therefore, if the deposition of SPs in the brain can be measured noninvasively, subjects who are certain to develop AD (i.e., "preclinical AD") could be screened as candidates for preventive therapy.

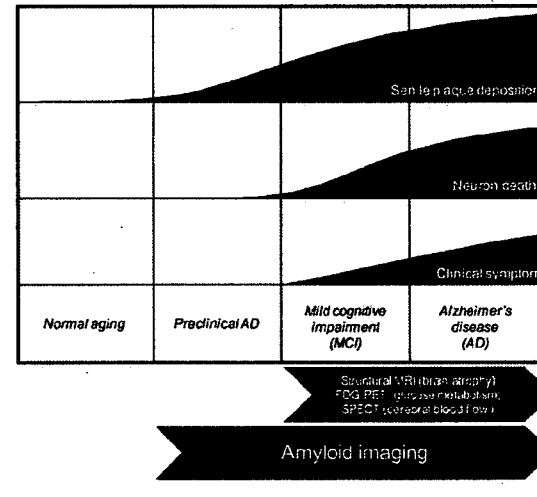

Fig. (1). Senile plaque deposition, neuron death and clinical symptom of Alzheimer's disease.

Recently, several imaging techniques, including positron emission tomography (PET), single photon emission computed tomography (SPECT), magnetic resonance imaging, and near-infrared imaging, have been developed for the noninvasive detection of SPs in AD patients. These techniques, recently classified as "amyloid imaging", are considered ideal for screening candidates for anti-amyloid therapy. PET is the most popular method for amyloid

*Address correspondence to this author at the Department of Pharmacology, Tohoku University School of Medicine, 2-1, Seiryo-machi, Aoba-ku, Sendai 980-8575, Japan; Tel: + 81-22-717-8058; Fax: +81-22-717-8060; E-mail: oka@mail.tains.tohoku.ac.jp

1573-4056/08 $55.00+.00

imaging, because of its advantages of high sensitivity, good spatial resolution, quantitative results, and ease of probe development.

DEVELOPMENT OF AMYLOID-IMAGING AGENTS

Recent advances in molecular imaging have enabled the noninvasive detection of amyloid deposits by PET or SPECT. For the high-contrast detection of amyloid deposits, imaging agents should have high binding affinity for Aβ fibrils and substantial permeability through the blood–brain barrier (BBB). Several amyloid-binding agents have been developed for the *in vivo* detection of amyloid deposits (Fig. (2)). The development of these agents started with the use of Congo red, which is commonly used for the histochemical staining of amyloid [4]. However, the BBB permeability of Congo red is limited because of its molecular size and electrostatic charge. Therefore, several Congo red derivatives have been developed with improved BBB permeability without reduced binding to amyloid [5-8]. Chrysamine-G is the first Congo red derivative that has been examined as an *in vivo* amyloid-imaging probe. However, entry of this compound into the brain is limited. Other derivatives, including BSB, ISB, and methoxy-X04, have also been developed to improve the BBB permeability. BSB successfully visualizes brain amyloid deposits in APP-transgenic mice after intravenous administration of the compound. However, this compound has insufficient BBB permeability for it to be useful as a clinical PET tracer. The first successful amyloid imaging agent to have been administered to humans is 2-(1-{6-[(2-[^{18}F]fluoroethyl)(methyl)amino]-2-naphthyl}ethylidene)malononitrile ([^{18}F]FDDNP) [9]. One of the characteristics of this agent is its ability to bind both SPs and NFTs in the AD brain. In addition, this compound is extremely lipophilic; therefore, it can penetrate the BBB more easily than previously reported compounds [10]. Interestingly, this compound binds to the same site in Aβ fibrils as non-steroidal anti-inflammatory drugs (NSAIDs) do. Therefore, this agent enables us to determine the occupancy rate of NSAIDs and experimental drugs in SPs [11]. Other candidate amyloid-imaging agents include thioflavin-T derivatives [12, 13]. N-methyl-[^{11}C]2-(4'-methylaminophenyl)-6-hydroxybenzothiazole ([^{11}C]PIB) is one such derivative and is currently the most successful amyloid-imaging agent. This compound shows high binding affinity for Aβ fibrils and SPs in AD brain homogenates, in contrast to low binding affinity for NFTs [14]. After intravenous administration, this agent shows high BBB permeability and rapid washout from normal brain tissue. Other amyloid-imaging agents, such as IMPY, stilbene, benzofuran, and acridine orange derivatives, have also been explored for use as PET and SPECT imaging probes [15-19]. The iodinated agent IMPY has been explored as a SPECT

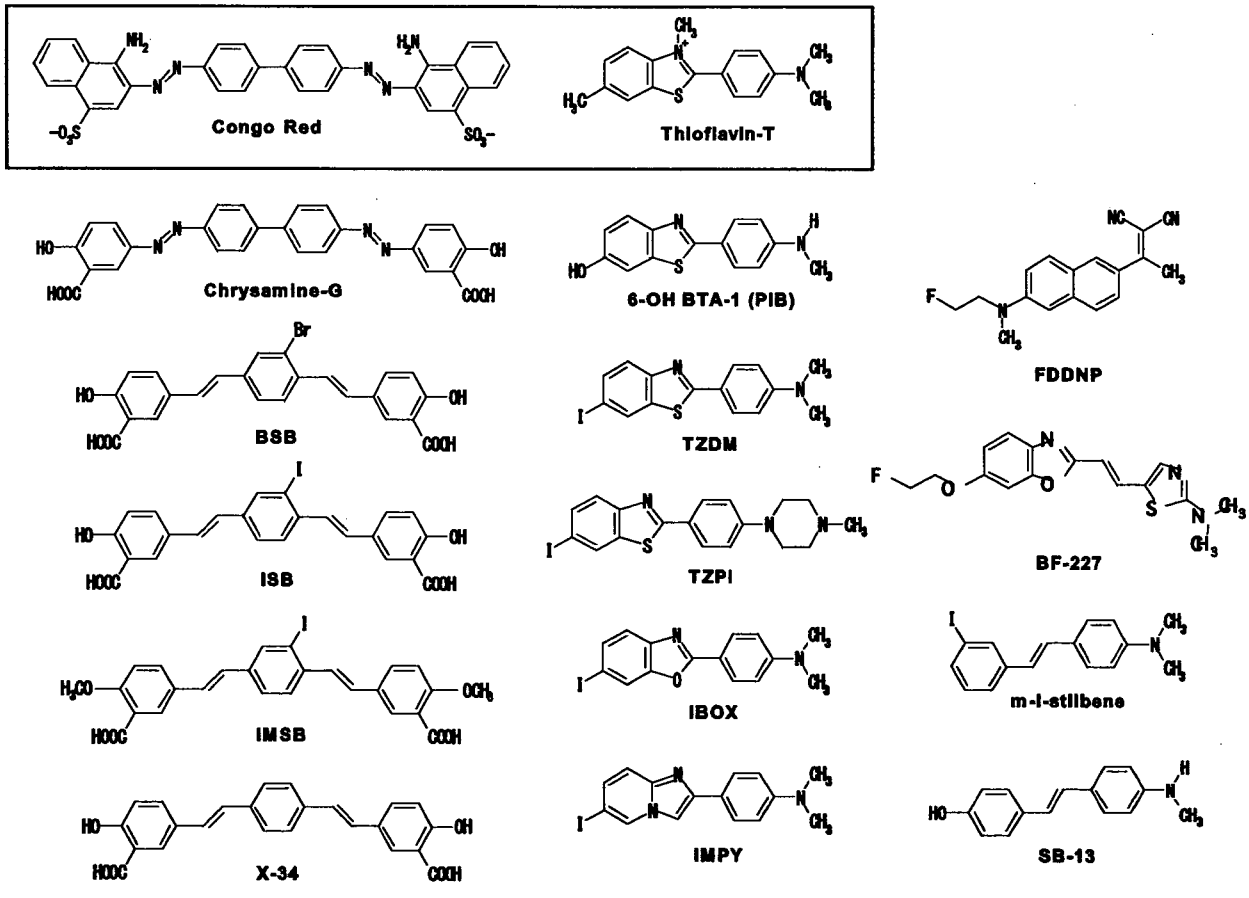

Fig. (2). Chemical structures of common imaging probes for amyloid plaques.

imaging agent and has been used in humans. Other iodinated agents are also under evaluation.

Benzoxazole derivatives are other possible amyloid-imaging agents [20-23]. Their chemical structures, binding affinities for Aβ fibrils, and pharmacokinetic data are summarized in Table 1. Most of these compounds show high binding affinity for both Aβ1-40 and Aβ1-42 fibrils. BF-191 and BF-208, which have halogens as substituents for amino groups, show low affinity for both Aβ1-40 and Aβ1-42 fibrils, suggesting that amino groups have a crucial role in binding to Aβ fibrils. All compounds have good BBB permeability. BF-227 shows faster washout from normal brain tissue than the other compounds [23, 24]. BF-227 distinctly stained SPs during the neuropathological staining of AD brain sections, and this staining pattern correlated well with Aβ immunostaining (Fig. (3)). Fluorescence microscopy revealed that this agent binds preferentially to SPs rather than NFTs. An acute and subacute toxicity study of BF-227 indicated sufficient safety for clinical use as a PET probe.

HUMAN PET STUDY

Human amyloid imaging was first studied using [^{18}F] FDDNP [9]. A [^{18}F]FDDNP PET study revealed regional accumulation of [^{18}F]FDDNP in the SP- and NFT-rich areas of the brain [25]. Global FDDNP-PET binding distinctly differentiated AD patients from normal subjects. FDDNP retention in the medial temporal lobes of subjects with mild cognitive impairment (MCI) was intermediate between levels in AD patients and normal control subjects. This finding is consistent with the observation in an autopsy study that the concentration of NFTs in the medial temporal lobes was intermediate between that in normally aging subjects and AD patients [26]. These binding characteristics indicate that this imaging agent is useful in tracing the progression of AD from the MCI stage. In addition, this agent has the potential to differentiate atypical prion disease from AD [27]. The weakness of this agent is the low signal-to-background ratio of the images, which is due to the considerable amount of nonspecific accumulation in normal brain tissue [28].

In comparison with [^{18}F]FDDNP, [^{11}C]PIB PET images differentiated AD patients from normal individuals more distinctly [29]. PIB retention was observed in the SP-rich neocortex of the brain but not in the NFT-rich medial temporal cortex, indicating that this agent binds selectively to SPs. A quantitative imaging method using PIB has already been validated [30, 31]. Over half the subjects with MCI also showed neocortical PIB accumulation to the same level as AD patients [32, 33]. Interestingly, MCI subjects who at clinical follow-up converted to AD showed higher PIB retention than subjects with non-progressive MCI, indicating that neocortical PIB retention is a marker for the prediction of progression to AD in the MCI stage [34]. A PIB-PET study in a nondemented population revealed elevated cortical retention of PIB in four nondemented persons [35]. These nondemented PIB-positive cases additionally showed an abnormality in the concentration of Aβ1-42 in cerebrospinal fluid, suggesting the presence of SPs in the absence of cognitive impairment [36]. There was a strong relationship between impaired memory performance and PIB binding in the nondemented population [37]. These findings suggest that amyloid imaging may be sensitive enough for the detection of a preclinical AD state. However, one should be careful when assessing abnormalities in the distribution of PIB, because PIB retention is also observed in cerebral amyloid angiopathy [38, 39]. Amyloid imaging may be useful as a surrogate marker for monitoring brain amyloid deposition during anti-amyloid therapy. However, longitudinal PIB-PET evaluation indicated relatively stable PIB retention after 2 years of follow-up in AD patients, suggesting that brain amyloid deposition reflected by PIB retention reaches a plateau at the early clinical stages of AD [40]. Therefore, therapy that retards the synthesis of Aβ (e.g., β- and γ-secretase inhibitors) should be started before the retention of amyloid-imaging tracers reaches a plateau.

The stilbene derivative SB-13 has also been used in a human PET study [41]. In a PET study, [^{11}C]SB-13 exhibited similar binding properties to PIB. For expanded use in clinical investigations, an ^{18}F-labeled stilbene derivative is under investigation.

A PET study using [^{11}C]BF-227 was performed at Tohoku University [23]. Neocortical retention of BF-227 was observed in an AD patient (Fig. (4)). A subject with MCI also showed cortical retention of BF-227. Interestingly, this subject was confirmed to progress to AD during the follow-up period, suggesting that cortical retention of BF-227 indicates a high risk of conversion to AD in MCI subjects. Several MCI subjects showed a distribution of BF-227 similar to that in normally aged subjects. All Alzheimer's patients and about 60% of MCI subjects showed an elevated standardized uptake value (SUV) ratio in the neocortical regions. Even in MCI subjects showing prominent retention of BF-227, the neocortical SUV ratio was below the mean value observed in AD patients. This finding suggests that MCI is a pathologically transitional state between normal aging and dementia, and that the amyloid deposition reflected by BF-227 retention does not reach a plateau in the MCI stage. Voxel-by-voxel analysis of BF-227 PET images demonstrated higher retention of BF-227 in the temporoparietal region in AD patients [23]. The pattern of distribution resembles the distribution of neuritic plaques in postmortem AD brains [42, 43]. Microscopic observation also indicates preferential binding of BF-227 to neuritic plaques in AD brain sections (Fig. (3)). In an *in vitro* binding experiment, BF-227 binding to Aβ increased linearly with increasing Aβ fibril formation [24]. For these reasons, BF-227 is considered to bind neuritic plaques selectively *in vivo*. A validation study is required to determine whether the retention of BF-227 in the neocortex accurately reflects the level of neuritic plaques rather than the level of diffuse plaques.

FUTURE DIRECTION OF PROBE DEVELOPMENT

The commercialization of ^{18}F-labeled agents or SPECT imaging agents is necessary for the wide clinical application of amyloid imaging. Because of the limited half-life of ^{11}C (20 min), the supply of ^{11}C-labeled PET agents is limited to facilities with an on-site cyclotron. ^{18}F-labeled agents are generally easier for routine clinical use because of the longer half-life of ^{18}F (110 min). Currently, several ^{18}F-labeled agents for amyloid imaging are under clinical evaluation. To

Table 1. Binding Affinity of Benzoxazole Derivatives for Aβ Fibrils and Brain Uptakes After Intravenous Administration in Normal Mice

Compounds	Chemical structure	Kd or Ki (nM)		Brain uptake (%ID/g)	
		Aβ1-40	Aβ1-42	2 min	30 min
BF-125	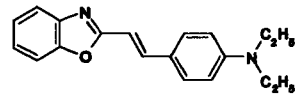	1.5 ± 0.76	4.9 ± 1.9	3.0 ± 0.87	3.0 ± 0.53
BF-133	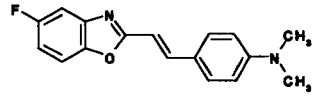	2.1 ± 1.1	3.4 ± 0.73	5.5 ± 0.40	3.8 ± 0.030
BF-140	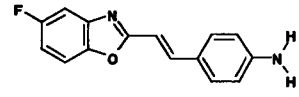	4.7 ± 2.2	2.1 ± 0.18	5.5 ± 0.60	1.1 ± 0.076
BF-145	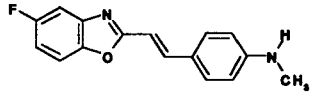	3.0 ± 0.46	4.5 ± 1.9	4.4 ± 1.80	1.6 ± 0.40
BF-168	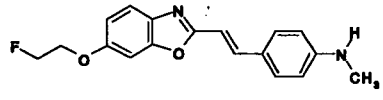	2.5 ± 2.3	6.4 ± 1.0	3.9 ± 0.22	1.6 ± 0.0071
BF-180	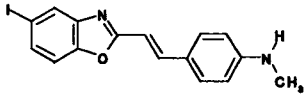	6.8 ± 1.4	10.6 ± 1.5	2.4 ± 0.52	1.8 ± 0.010
BF-185	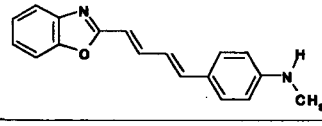	2.5 ± 2.3	14 ± 10	3.9 ± 0.49	3.8 ± 0.16
BF-191	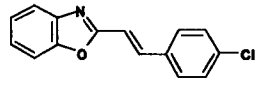	> 5000	> 5000	12 ± 0.26	1.7 ± 0.16
BF-208	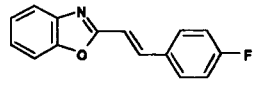	> 5000	> 5000	5.6 ± 0.64	0.28 ± 0.024
BF-227	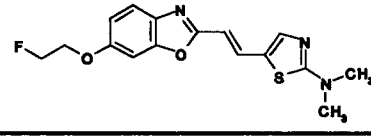	1.8 ± 0.42	4.3 ± 1.5	7.9 ± 0.18	0.54 ± 0.029

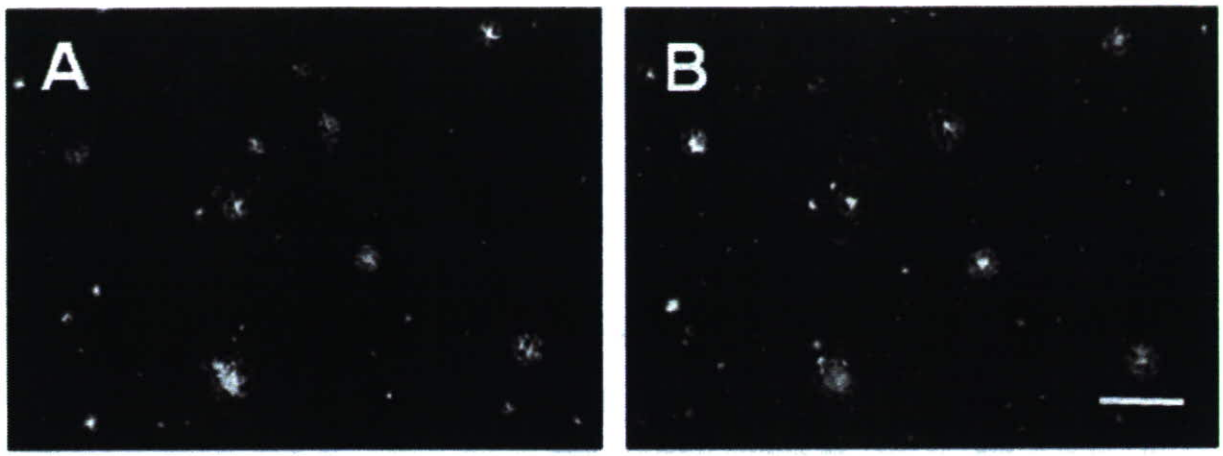

Fig. (3). Fluorescence microscopic images of senile plaques in Alzheimer's disease using BF-227 (A) and Aβ specific antibody 6F/3D (B) Bar = 100μm.

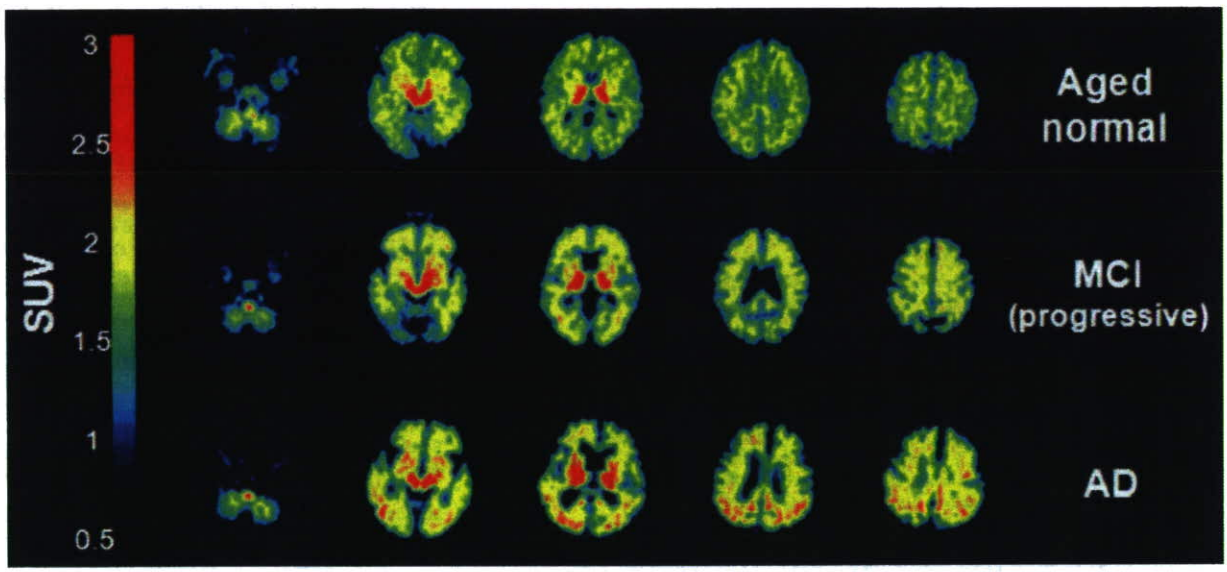

Fig. (4). Mean SUV images between 20 and 40 min post-injection of [^{11}C]BF-227 in aged normal, MCI and AD cases.

obtain a better understanding of the pathophysiology of AD, it is also necessary to visualize the distributions of Aβ pathology and tau pathology individually. However, no surrogate markers are available for evaluating the deposition of NFTs in the brain, because of the difficulty in developing a tau-specific imaging probe [44]. We previously introduced the novel compounds BF-126 and BF-170 as candidates for tau imaging [45]. In AD brain sections, BF-126 and BF-170 visualize NFTs, neuropil threads, and PHF-type neuritis distinctly. For clinical application, optimization of these compounds to reduce non-specific binding is in progress.

CONCLUSION

Several amyloid-imaging agents have been successfully developed for PET imaging. These agents displayed high binding affinity for Aβ fibrils and high BBB permeability. [^{11}C]PIB, [^{18}F]FDDNP, and [^{11}C]BF-227 displayed selective *in vivo* binding to amyloid in the brain and clearly differentiated early AD patients from normal populations. The development of ^{18}F-labeled agents or SPECT imaging agents is necessary for the wide application of amyloid imaging. The development of an NFT-specific imaging agent is also much needed. Amyloid imaging is currently the best method for the early and accurate diagnosis of AD and for monitoring amyloid pathology in the brain. This imaging technology and the forthcoming anti-amyloid therapy will cooperatively contribute to the prevention of dementia.

ACKNOWLEDGEMENTS

This study was partially supported by the Special Coordination Funds for Promoting Science and Technology, the Program for the Promotion of Fundamental Studies in Health Science of the National Institute of Biomedical Innovation, the Industrial Technology Research Grant

Program of the New Energy and Industrial Technology Development Organization (NEDO) of Japan, Health and Labour Sciences Research Grants for Translational Research from the Japanese Ministry of Health, Labour and Welfare, and a JST grant for research and education in molecular imaging.

DISCLOSURE STATEMENT

All authors have no conflict of interest.

REFERENCES

[1] Tanzi RE, Bertram L. Twenty years of the Alzheimer's disease amyloid hypothesis: a genetic perspective. Cell 2005; 120: 545-555.

[2] Goldman WP, Price JL, Storandt M, *et al.* Absence of cognitive impairment or decline in preclinical Alzheimer's disease. Neurology 2001; 56: 361-367.

[3] Price JL, Morris JC. Tangles and plaques in nondemented aging and "preclinical" Alzheimer's disease. Ann Neurol 1999; 45: 358-368.

[4] Klunk WE, Debnath ML, Pettegrew JW. Development of small molecule probes for the beta-amyloid protein of Alzheimer's disease. Neurobiol Aging 1994; 691-698.

[5] Klunk WE, Debnath ML, Pettegrew JW. Chrysamine-G binding to Alzheimer and control brain: autopsy study of a new amyloid probe. Neurobiol Aging 1995; 16: 541-548.

[6] Skovronsky DM, Zhang B, Kung MP, Kung HF, Trojanowski JQ, Lee VM. *In vivo* detection of amyloid plaques in a mouse model of Alzheimer's disease. Proc Natl Acad Sci USA 2000; 97: 7609-7614.

[7] Zhuang ZP, Kung MP, Hou C, *et al.* Radioiodinated styrylbenzenes and thioflavins as probes for amyloid aggregates. J Med Chem 2001; 44: 1905-1914.

[8] Klunk WE, Bacskai BJ, Mathis CA, *et al.* Imaging Abeta plaques in living transgenic mice with multiphoton microscopy and methoxy-X04, a systemically administered Congo red derivative. J Neuropathol Exp Neurol 2002; 61: 797-805.

[9] Shoghi-Jadid K, Small GW, Agdeppa ED, *et al.* Localization of neurofibrillary tangles and beta-amyloid plaques in the brains of living patients with Alzheimer disease. Am J Geriatr Psychiatry 2002; 10: 24-35.

[10] Agdeppa ED, Kepe V, Liu J, *et al.* Binding characteristics of radiofluorinated 6-dialkylamino-2-naphthylethylidene derivatives as positron emission tomography imaging probes for beta-amyloid plaques in Alzheimer's disease. J Neurosci 2001; 21: RC189.

[11] Agdeppa ED, Kepe V, Petri A, *et al. In vitro* detection of (S)-naproxen and ibuprofen binding to plaques in the Alzheimer's brain using the positron emission tomography molecular imaging probe 2-(1-[6-[(2-[(18)F]fluoroethyl)(methyl) amino]-2-naphthyl]ethylidene)malononitrile. Neuroscience 2003; 117: 723-730.

[12] Mathis CA, Wang Y, Klunk WE. Imaging beta-amyloid plaques and neurofibrillary tangles in the aging human brain. Curr Pharm Des 2004; 10: 1469-1492.

[13] Klunk WE, Wang Y, Huang GF, Debnath ML, Holt DP, Mathis CA. Uncharged thioflavin-T derivatives bind to amyloid-beta protein with high affinity and readily enter the brain. Life Sci 2001; 69: 1471-1484.

[14] Klunk WE, Wang Y, Huang GF, *et al.* The binding of 2-(4'-methylaminophenyl)benzothiazole to postmortem brain homogenates is dominated by the amyloid component. J Neurosci 2003; 23: 2086-2092.

[15] Kung MP, Hou C, Zhuang ZP, *et al.* IMPY: an improved thioflavin-T derivative for *in vivo* labeling of beta-amyloid plaques. Brain Res 2002; 956: 202-210.

[16] Kung HF, Kung MP, Zhuang ZP, *et al.* Iodinated tracers for imaging amyloid plaques in the brain. Mol Imaging Biol 2003; 5: 418-426.

[17] Ono M, Wilson A, Nobrega J, *et al.* ^{11}C-labeled stilbene derivatives as Abeta-aggregate-specific PET imaging agents for Alzheimer's disease. Nucl Med Biol 2003; 30: 565-571.

[18] Ono M, Kawashima H, Nonaka A, *et al.* Novel benzofuran derivatives for PET imaging of beta-amyloid plaques in Alzheimer's disease brains. J Med Chem 2006; 49: 2725-2730.

[19] Suemoto T, Okamura N, Shiomitsu T, *et al. In vivo* labeling of amyloid with BF-108. Neurosci Res 2004; 48: 65-74.

[20] Okamura N, Suemoto T, Shimadzu H, *et al.* Styrylbenzoxazole derivatives for *in vivo* imaging of amyloid plaques in the brain. J Neurosci 2004; 24: 2535-2541.

[21] Okamura N, Suemoto T, Shiomitsu T, *et al.* A novel imaging probe for *in vivo* detection of neuritic and diffuse amyloid plaques in the brain. J Mol Neurosci 2004; 24: 247-255.

[22] Furumoto S, Okamura N, Iwata R, Yanai K, Arai H, Kudo Y. Recent advances in the development of amyloid imaging agents. Curr Top Med Chem 2007; 7: 1773-1789.

[23] Kudo Y, Okamura N, Furumoto S, *et al.* 2-(2-[2-Dimethylaminothiazol-5-yl]ethenyl)-6- (2-[fluoro]ethoxy)benzoxazole: a novel PET agent for *in vivo* detection of dense amyloid plaques in Alzheimer's disease patients. J Nucl Med 2007; 48: 553-561.

[24] Okamura N, Furumoto S, Funaki Y, *et al.* Binding and safety profile of novel benzoxazole derivative for *in vivo* imaging of amyloid deposits in Alzheimer's disease. Geriatr Gerontol Int 2007 (in press)

[25] Small GW, Kepe V, Ercoli LM, *et al.* PET of brain amyloid and tau in mild cognitive impairment. N Engl J Med 2006; 355: 2652-2663.

[26] Petersen RC, Parisi JE, Dickson DW, *et al.* Neuropathologic features of amnestic mild cognitive impairment. Arch Neurol 2006; 63: 665-672.

[27] Boxer AL, Rabinovici GD, Kepe V, *et al.* Amyloid imaging in distinguishing atypical prion disease from Alzheimer disease. Neurology 2007; 69: 283-290.

[28] Bacskai BJ, Klunk WE, Mathis CA, Hyman BT. Imaging amyloid-beta deposits *in vivo*. J Cereb Blood Flow Metab 2002; 22: 1035-1041.

[29] Klunk WE, Engler H, Nordberg A, *et al.* Imaging brain amyloid in Alzheimer's disease with Pittsburgh Compound-B. Ann Neurol 2004; 55: 306-319.

[30] Price JC, Klunk WE, Lopresti BJ, *et al.* Kinetic modeling of amyloid binding in humans using PET imaging and Pittsburgh Compound-B. J Cereb Blood Flow Metab 2005; 25: 1528-1547.

[31] Lopresti BJ, Klunk WE, Mathis CA, *et al.* Simplified quantification of Pittsburgh Compound B amyloid imaging PET studies: a comparative analysis. J Nucl Med 2005; 46: 1959-1972.

[32] Rowe CC, Ng S, Ackermann U, *et al.* Imaging beta-amyloid burden in aging and dementia. Neurology. 2007; 68: 1718-1725.

[33] Kemppainen NM, Aalto S, Wilson IA, *et al.* PET amyloid ligand [^{11}C]PIB uptake is increased in mild cognitive impairment. Neurology 2007; 68: 1603-1606.

[34] Forsberg A, Engler H, Almkvist O, *et al.* PET imaging of amyloid deposition in patients with mild cognitive impairment. Neurobiol Aging 2007 (in press)

[35] Mintun MA, Larossa GN, Sheline YI, *et al.* [^{11}C]PIB in a nondemented population: potential antecedent marker of Alzheimer disease. Neurology 2006; 67: 446-452.

[36] Fagan AM, Mintun MA, Mach RH, *et al.* Inverse relation between *in vivo* amyloid imaging load and cerebrospinal fluid Abeta42 in humans. Ann Neurol 2006; 59: 512-519.

[37] Pike KE, Savage G, Villemagne VL, *et al.* Beta-amyloid imaging and memory in non-demented individuals: evidence for preclinical Alzheimer's disease. Brain 2007; 130: 2837-2844.

[38] Bacskai BJ, Frosch MP, Freeman SH, *et al.* Molecular imaging with Pittsburgh Compound B confirmed at autopsy: a case report. Arch Neurol 2007; 64: 431-434.

[39] Johnson KA, Gregas M, Becker JA, *et al.* Imaging of amyloid burden and distribution in cerebral amyloid angiopathy. Ann Neurol 2007; 62: 229-234.

[40] Engler H, Forsberg A, Almkvist O, *et al.* Two-year follow-up of amyloid deposition in patients with Alzheimer's disease. Brain 2006; 129: 2856-2866.

[41] Verhoeff NP, Wilson AA, Takeshita S, *et al.* In-vivo imaging of Alzheimer disease beta-amyloid with [^{11}C]SB-13 PET. Am J Geriatr Psychiatry 2004; 12: 584-595.

[42] Arnold SE, Hyman BT, Flory J, Damasio AR, Van Hoesen GW. The topographical and neuroanatomical distribution of neurofibrillary tangles and neuritic plaques in the cerebral cortex of patients with Alzheimer's disease. Cereb Cortex 1991; 1: 103-116.

[43] Cummings JL, Cole G. Alzheimer disease. JAMA 2002; 287: 2335-2338.

[44] Small GW, Agdeppa ED, Kepe V, Satyamurthy N, Huang SC, Barrio JR. *In vivo* brain imaging of tangle burden in humans. J Mol Neurosci 2002; 19: 323-327.

[45] Okamura N, Suemoto T, Furumoto S, *et al.* Quinoline and benzimidazole derivatives: candidate probes for *in vivo* imaging of tau pathology in Alzheimer's disease. J Neurosci 2005; 25: 10857-10862.

Received: December 5, 2007 Revised: December 7, 2007 Accepted: December 10, 2007

2-(2-[2-Dimethylaminothiazol-5-yl]Ethenyl)-6-(2-[Fluoro]Ethoxy)Benzoxazole: A Novel PET Agent for In Vivo Detection of Dense Amyloid Plaques in Alzheimer's Disease Patients

Yukitsuka Kudo[1], Nobuyuki Okamura[2], Shozo Furumoto[1], Manabu Tashiro[3], Katsutoshi Furukawa[4], Masahiro Maruyama[4], Masatoshi Itoh[3], Ren Iwata[5], Kazuhiko Yanai[2], and Hirtoyuki Arai[4]

[1]Tohoku University Biomedical Engineering Research Organization (TUBERO), Sendai, Japan; [2]Department of Pharmacology, Tohoku University School of Medicine, Sendai, Japan; [3]Division of Cyclotron Nuclear Medicine, Cyclotron and Radioisotope Center, Tohoku University, Sendai, Japan; [4]Department of Geriatrics and Gerontology, Center for Asian Traditional Medicine, Tohoku University School of Medicine, Sendai, Japan; and [5]Division of Radiopharmaceutical Chemistry, Cyclotron and Radioisotope Center, Tohoku University, Sendai, Japan

Extensive deposition of dense amyloid fibrils is a characteristic neuropathologic hallmark in Alzheimer's disease (AD). Noninvasive detection of these molecules is potentially useful for early and precise detection of patients with AD. This study reports a novel compound, 2-(2-[2-dimethylaminothiazol-5-yl]ethenyl)-6-(2-[fluoro]ethoxy)benzoxazole (BF-227), for in vivo detection of dense amyloid deposits using PET. **Methods:** The binding affinity of BF-227 to amyloid-β (Aβ) fibrils was calculated. The binding property of BF-227 to amyloid plaques was evaluated by neuropathologic staining of AD brain sections. Brain uptake and in vivo binding of BF-227 to Aβ deposits were also evaluated using mice. For clinical evaluation of ^{11}C-BF-227 as a PET probe, 11 normal (healthy) subjects and 10 patients with AD participated in this study. Dynamic PET images were obtained for 60 min after administration of ^{11}C-BF-227. The regional standardized uptake value (SUV) and the ratio of regional to cerebellar SUV were calculated as an index of ^{11}C-BF-227 retention. The regional tracer distribution in AD patients was statistically compared with that of aged normal subjects on a voxel-by-voxel basis. **Results:** BF-227 displayed high binding affinity to synthetic Aβ1-42 fibrils (K_i [inhibition constant], 4.3 ± 1.5 nM). Neuropathologic staining has demonstrated preferential binding of this agent to dense amyloid deposits in AD brain. Moreover, a biodistribution study of this agent revealed excellent brain uptake and specific labeling of amyloid deposits in transgenic mice. The present clinical PET study using ^{11}C-BF-227 demonstrated the retention of this tracer in cerebral cortices of AD patients but not in those of normal subjects. All AD patients were clearly distinguishable from normal individuals using the temporal SUV ratio. Voxel-by-voxel analysis of PET images revealed that cortical BF-227 retention in AD patients is distributed primarily to the posterior association area of the brain and corresponded well with the preferred site for neuritic plaque depositions containing dense Aβ fibrils. **Conclusion:** These findings suggest that BF-227 is a promising PET probe for in vivo detection of dense amyloid deposits in AD patients.

J Nucl Med 2007; 48:553–561
DOI: 10.2967/jnumed.106.037556

Substantial neuropathologic evidence suggests that the deposition of senile plaques (SPs) and neurofibrillary tangles (NFTs) represents the characteristic neuropathologic hallmark in Alzheimer's disease (AD) (*1*). Progressive accumulation of SPs is considered fundamental to the initial development of dementia. Extensive deposition of SPs in the brain is present even in very mild AD and precedes the presentation of cognitive impairment (*2,3*). Several antiamyloid drugs are under development for the treatment and prevention of AD (*4*). For early detection and preventive intervention for AD, noninvasive imaging of neuropathologic lesions is a powerful strategy.

For this purpose, several imaging techniques have been developed that can noninvasively detect SPs in the brain using PET, SPECT, and MRI. Among these imaging modalities, PET is the most advanced and practical method for in vivo measurement of SP depositions. To achieve successful imaging using PET, various radiolabeled agents have been developed. Currently, 6OH-BTA-1 (PIB) is the most successful PET agent for in vivo amyloid imaging. This tracer sensitively detects amyloid fibrils in the brain and is proven to be useful for early diagnosis of AD (*5–7*).

However, amyloid-β (Aβ) deposition is also frequent in aging, even in cognitively intact individuals. Excessive identification of Aβ has a potential risk to misjudge the normal aging process with abnormal Aβ deposition. In the

Received Oct. 23, 2006; revision accepted Jan. 20, 2007.
For correspondence or reprints contact: Nobuyuki Okamura, MD, Department of Pharmacology, Tohoku University School of Medicine, 2-1, Seiryo-machi, Aoba-ku, Sendai 980-8575, Japan.
E-mail: oka@mail.tains.tohoku.ac.jp

normal aging process, noncompact or diffuse amyloid plaques containing less fibrillar Aβ are deposited primarily in the brain. Brains from patients with AD are characterized by an anatomically widespread process of amyloid deposition and neuritic plaque formation containing dense amyloid fibrils (*8*). A shift of brain Aβ from the soluble to the fibrillar form is closely associated with the onset of AD (*9*). Therefore, selective detection of dense amyloid fibrils would be advantageous to differentiate the normal aging process from AD with high specificity.

We have previously demonstrated a novel series of benzoxazole derivatives as promising candidates for an in vivo imaging probe of SPs (*10–12*). These derivatives showed comparatively high blood–brain barrier (BBB) permeability, high binding affinity for Aβ aggregates, and high specificity for fibrillar Aβ deposits, suggesting potential merit for the early detection of AD-related pathologies. Herein we introduce an optimized derivative, 2-(2-[2-dimethylaminothiazol-5-yl]ethenyl)-6-(2-[fluoro]ethoxy)benzoxazole (BF-227), as a PET probe for in vivo detection of dense amyloid deposits in humans.

MATERIALS AND METHODS

Preparation of Compounds

BF-227 (Fig. 1) and its *N*-desmethylated derivative (a precursor of ^{11}C-BF-227) were custom-synthesized by Tanabe R&D Service Co. ^{11}C-BF-227 was synthesized from the precursor by *N*-methylation in dimethyl sulfoxide (Fig. 1) using ^{11}C-methyl triflate (*13,14*). After quenching the reaction with 5% acetic acid in ethanol, ^{11}C-BF-227 was separated from the crude mixture by semipreparative reversed-phase high-performance liquid chromatography and then isolated from the collected fraction by solid-phase extraction. The purified ^{11}C-BF-227 was solubilized in isotonic saline containing 1% polysobate-80 and 5% ascorbic acid. The saline solution was filter-sterilized with a 0.22-μm Millipore filter for clinical use. The radiochemical yields were >50% based on ^{11}C-methyl triflate, and the specific radioactivities were 119–138 GBq/μmol at the end of synthesis. The radiochemical purities were >95%.

In Vitro Binding Assays

Binding affinities of the compounds for synthetic Aβ1-42 aggregates were examined as described previously (*10*). Briefly, solid-form Aβ1-42 (Peptide Institute) was dissolved in 10 mM potassium phosphate buffer (pH 7.4) and incubated at 37°C for 40 h. The binding assay was performed by mixing 100 μL of aggregated Aβ1-42 with the appropriate concentration of ^{125}I-labeled 2-(4-methylamino)styryl-5-iodo-benzoxazole (BF-180) and 8% ethanol. After incubation for 4 h at room temperature, the binding mixture was filtered and filters containing bound ^{125}I ligand were counted using a γ-counter. The dissociation constant (K_d) and maximum specific binding (B_{max}) of BF-180 were determined. For inhibition studies, binding studies were performed using synthetic Aβ1-42 aggregates. A mixture containing 50 μL of BF-227, 50 μL of 0.05 nM ^{125}I-BF-180, 100 μL of 100 nM Aβ1–42, and 800 μL of 8% ethanol was incubated at room temperature for 4 h. The mixture was then filtered through Whatman GF/B filters, and filters containing bound ^{125}I ligand were counted in a γ-counter. Values for the half-maximal inhibitory concentration (IC_{50}) were determined from displacement curves of 3 independent experiments using Prism software (GraphPad), and values for the inhibition constant (K_i) were determined using the Cheng–Prusoff equation.

Measurement of Octanol/Water Partition Coefficients

Phosphate-buffered saline (PBS) and 1-octanol (Wako) were saturated with 1-octanol and PBS, respectively, before use. BF-227 was dissolved in 1-octanol and shaken with equal amounts of PBS for 30 min at room temperature. After centrifugation at 2,000 rpm for 15 min, absorbency of the 1-octanol layer was measured at the peak wavelength of the absorbance spectrum of BF-227 using a Spectra Max 190 microplate reader (Molecular Devices). Octanol/water partition coefficients were determined by comparing absorbency with that before shaking with PBS. Each data point was performed in duplicate.

BBB Permeability of BF-227 in Normal Mice

Brain uptake of BF-227 was measured using ^{11}C-labeled compound. The ^{11}C-BF-227 (1.1–6.3 MBq) was administered into the tail vein of male C57B6 mice (n = 23; mean weight, 28–32 g). Mice were then sacrificed by decapitation at 2, 10, 30, and 60 min after injection. The whole brain was removed and weighed, and radioactivity was counted using an automatic γ-counter. The percentage injected dose per gram of tissue (%ID/g) was calculated by normalizing tissue counts to tissue weight. Each %ID/g value is expressed as a mean ± SD of 3 or 4 separate experiments.

Neuropathologic Staining

Postmortem brain tissues from a 69-y-old man with autopsy-confirmed AD and an 81-y-old man with autopsy-confirmed physiologic aging were obtained from Fukushimura Hospital (Toyohashi, Japan). Experiments were performed under the regulations of the ethics committee of BF Research Institute. Serial sections (6-μm thick) from paraffin-embedded blocks of temporal cortex, striatum, and cerebellum were prepared in xylene and ethanol. Before

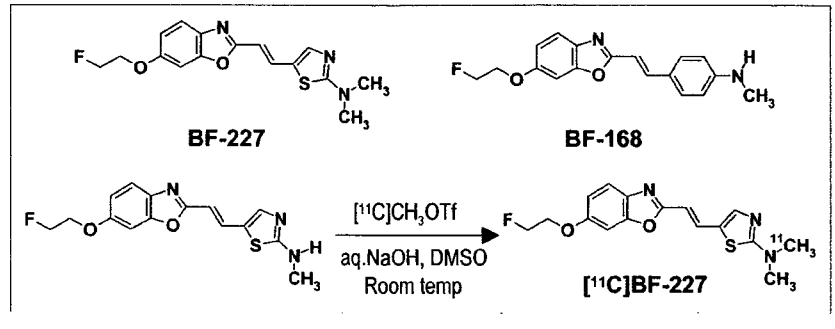

FIGURE 1. Chemical structures of BF-227 and BF-168 and radiosynthesis of BF-227.

the staining of compounds, quenching of autofluorescence was performed as described previously. Quenched tissue sections were immersed in 100 μM of BF-227 or 0.125% thioflavin-S solution containing 50% ethanol for 10 min. Sections stained with each compound were then dipped briefly into water and rinsed in PBS for 60 min before coverslipping with Fluor Save Reagent (Calbiochem); sections were examined using an Eclipse E800 microscope (Nikon) equipped with a V-2A filter set (excitation, 380–420 nm; dichroic mirror, 430 nm; long-pass filter, 450 nm). Sections stained with thioflavin-S were dipped briefly in tap water and in 50% ethanol and then washed in PBS for 60 min before coverslipping; this was followed by fluorescent microscopy using a BV-2A filter set (excitation, 400–440 nm; dichroic mirror, 455 nm; long-pass filter, 470 nm). In addition, adjacent sections were immunostained using monoclonal antibody (mAb) against Aβ (6F/3D; Dako A/S). After pretreatment with 90% formic acid for 5 min, sections were immersed in blocking solution for 30 min and then incubated for 60 min at 37°C with 6F/3D at a dilution of 1:50. After incubation, sections were processed by the avidin–biotin method using a Pathostain ABC-POD(M) Kit (Wako) and diaminobenzidine tetrahydrochloride.

Labeling of Aβ Deposits in Transgenic Mouse Brain

Ex vivo plaque labeling with BF-227 was evaluated using PS1/APPsw double transgenic mice (n = 2) and a wild-type mouse (n = 1) (male, 32-wk old) (*15*). A BF-227 solution containing 10% polyethylenglycol 400 and 0.1 mol/L HCl was administered into the tail vein at a dose of 4 mg/kg. Mice were anesthetized using sodium pentobarbital 2 h after injection of BF-227; they were then perfused transcardially with ice-cold saline, which was followed by 4% paraformaldehyde in 0.1 M PBS, and the brains were removed. After cryoprotection in 30% sucrose/0.1 M PBS, 6-μm frozen sections were cut using an OTF cryostat and imaged with no additional staining for fluorescent microscopy using a V-2A filter set. The same sections were immunostained using mAb against Aβ (6F/3D) as described earlier.

Subjects and Patients in Clinical PET Study

Eleven normal (healthy) control subjects, including 3 young normal subjects and 8 aged-matched normal subjects, and 10 probable AD patients underwent PET measurement of ^{11}C-BF-227 distribution in the brain (Table 1). AD patients were recruited through the Tohoku University Hospital Dementia Patients Registry. The diagnosis of AD was made according to the National Institute of Neurological and Communicative Diseases and Stroke/Alzheimer's Disease and Related Disorders Association (NINCDS–ADRDA) criteria. The normal control group was recruited from volunteers, who were taking no centrally acting medication, had no cognitive impairment, and had no cerebrovascular lesion on MR images. No significant difference in age was apparent between the AD group and the aged normal control group. AD patients had significantly lower mean mini-mental status examination (MMSE) scores than normal control subjects. This study was approved by the ethics committee on clinical investigations of Tohoku University School of Medicine and was performed in accordance with the Declaration of Helsinki. After complete description of the study to the patients and subjects, written informed consent was obtained.

Image Acquisition Protocols

The protocol of the PET study was approved by the Committee on Clinical Investigation at The Tohoku University School of Medicine and the Advisory Committee on Radioactive Substances at Tohoku University. The ^{11}C-BF-227 PET study was performed using a SET-2400W PET scanner (Shimadzu). After intravenous injection of 211–366 MBq of ^{11}C-BF-227, dynamic PET images were obtained for 60 min (23 sequential scans: 5 scans × 30 s, 5 scans × 60 s, 5 scans × 150 s, and 8 scans × 300 s) with each subject's eyes closed. The T1-weighted MR images were obtained using a SIGNA 1.5-T machine (GE Healthcare).

TABLE 1
Subject Demographics

Group	Subject	Sex	Age (y)	MMSE score
Young normal	YN 1	M	36	30
(n = 3)	YN 2	M	37	30
	YN 3	M	36	30
	Mean ± SD		36.3 ± 0.6	30.0 ± 0.0
Aged normal	AN 1	M	69	30
(n = 8)	AN 2	F	70	29
	AN 3	F	64	30
	AN 4	F	65	30
	AN 5	M	67	30
	AN 6	M	69	30
	AN 7	M	71	30
	AN 8	M	59	30
	Mean ± SD		66.8 ± 4.0	29.9 ± 0.4
All normal	Mean ± SD		58.5 ± 14.6	29.9 ± 0.3
(n = 11)				
AD (n = 10)	AD 1	F	65	24
	AD 2	M	75	19
	AD 3	F	72	21
	AD 4	F	82	18
	AD 5	F	62	20
	AD 6	F	68	21
	AD 7	M	70	23
	AD 8	F	85	23
	AD 9	M	78	14
	AD 10	F	75	26
	Mean ± SD		73.2 ± 7.3*	20.9 ± 3.4*†

*P < 0.05 vs. young normal group.
†P < 0.05 vs. aged normal group.
MMSE = mini-mental state examination.

Image Analysis

First, standardized uptake value (SUV) images of ^{11}C-BF-227 were obtained by normalizing tissue radioactivity concentration by injected dose and body weight. Subsequently, individual MR images were anatomically coregistered into individual PET images using Statistical Parametric Mapping software (SPM2; Wellcome Department, U.K.) (*16*). Regions of interest (ROIs) were placed on individual axial MR images in the cerebellar hemisphere, striatum, thalamus, frontal cortex (Brodmann's areas [BA] 8, 9, 10, 44, 45, 46, and 47), lateral temporal cortex (BA 21, 22, 37, and 38), parietal cortex (BA 39 and 40), temporooccipital cortex (BA 18 and 19), occipital cortex (BA 17), medial temporal cortex (BA 27, 28, 34, and 35), pons, and subcortical white matter, as described previously (*17*). The ROI information was then copied onto dynamic PET SUV images, and regional SUVs were sampled using Dr.View/LINUX software (Asahi-Kasei Joho System).

The interrater reliability for the ROI measurement was tested between 2 raters in 14 subjects and patients. The intraclass correlation coefficient was 0.95 in the frontal cortex and cerebellum, 0.97 in the lateral temporal and parietal cortices, and 0.98 in the medial temporal cortex. The correlation coefficient between these 2 measurements was 0.96 in the frontal cortex, 0.97 in the lateral temporal cortex, and 0.99 in the parietal cortex, medial temporal cortex, and cerebellum. SUVs between 40 and 60 min were averaged to calculate the SUVs for group comparison.

Statistical Analysis

For statistical comparison in the 3 groups, we applied the Kruskal–Wallis test, which was followed by Dunn's multiple comparison test. The difference in time–activity curves in ^{11}C-BF-227 PET was also evaluated by repeated measures ANOVA, which was followed by the Bonferroni–Dunn post hoc test. For statistical comparisons of PET measurements in aged normal and AD groups, we used the Mann–Whitney *U* test. Effect-size coefficients (Cohen's *d*) were also calculated for the evaluation of group differences in PET measurements. Statistical significance for each analysis was defined as $P < 0.05$. Statistical comparison between images from normal control subjects and AD patients was performed on a voxel-by-voxel basis using SPM2 software (*16*). SUV summation images 30–60 min after injection were stereotactically normalized using individual MR images into a standard space of Talairach and Tournoux. The normalized images were smoothed using a 16 × 16 × 16 mm gaussian filter. The count of each voxel was normalized to the cerebellar ROI value, because cerebellum is reported to be a region free of fibrillar amyloid plaques in AD brain. Images of patients with AD ($n = 10$) were compared with those of aged normal control subjects ($n = 8$) for between-group analysis ($P < 0.001$, uncorrected; extent threshold, $k = 200$). For the group analysis, a 2-sample *t* test was used to detect differences between the AD and normal control groups.

RESULTS

In Vitro Binding Study for Aβ Fibrils

In vitro binding assay indicated that BF-227 shows high binding affinity for Aβ1-42 fibrils. K_i for Aβ1-42 fibrils in competitive binding assay using ^{125}I-BF-180 was 4.3 ± 1.5 nM in BF-227, comparable to levels previously reported for compound BF-168.

Neuropathologic Staining in AD Brain Sections

Neuropathologic examination using BF-227 indicated that amyloid plaques were selectively stained with BF-227 in AD brain sections (Fig. 2A). Especially, cored plaques were brightly stained with BF-227, indicating that this compound preferentially binds to mature amyloid plaque. This staining pattern correlated well with Aβ immunostaining in adjacent sections (Fig. 2B, arrows). BF-227 staining was further compared with staining using thioflavin-S. In contrast to clear staining of SPs and NFTs with thioflavin-S (Fig. 2C), BF-227 primarily stained SPs, with faint staining of NFTs (Fig. 2B, arrowheads). No apparent staining was also observed in the temporal brain section of the aged normal case (Fig. 2D).

BBB Permeability and Clearance from Normal Brain

Next, we investigated whether BF-227 entered the brain in amounts sufficient for use as a PET agent. The log *P* value of BF-227 was 1.75, close to that of BF-168 (log $P = 1.79$). Intravenous administration of BF-227 into normal mice indicated that this compound readily penetrated the BBB. Brain uptakes at 2, 10, 30, and 60 min after intravenous injection of ^{11}C-BF-227 were 7.9 ± 1.3, 3.7 ± 0.37, 1.4 ± 0.36, and 0.64 ± 0.15 %ID/g, respectively. ^{11}C-BF-227 displayed double the initial uptake and faster washout

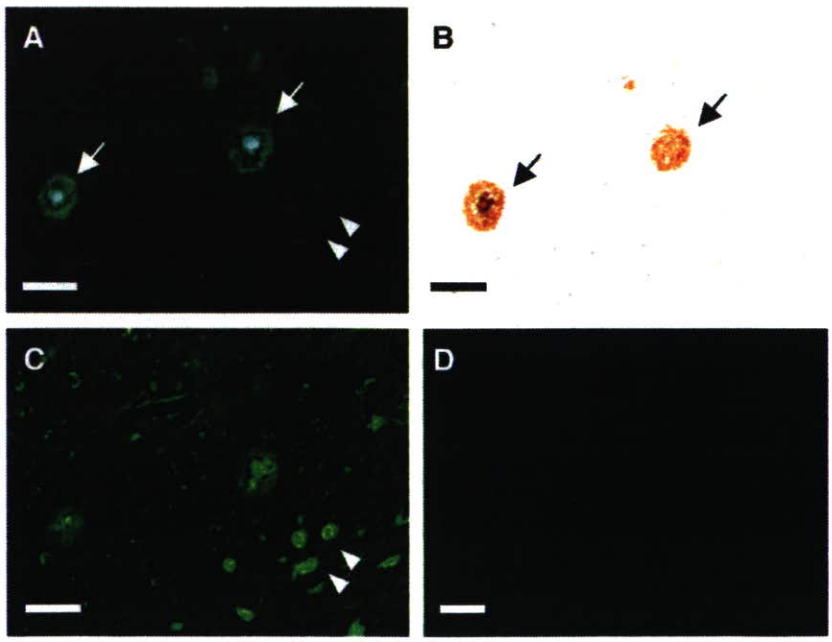

FIGURE 2. Neuropathologic staining of human brain sections by BF-227. Amyloid plaques are clearly stained with BF-227 in AD temporal brain sections (A). BF-227 staining correlates well with Aβ immunostaining in adjacent sections (B, arrows). BF-227 faintly stains NFTs, in contrast to clear staining with thioflavin-S (C, arrowheads). In aged normal temporal cortex (D), no staining by BF-227 is observed. Bar in A–C = 50 μm; bar in D = 200 μm.

in normal brain tissue compared with those of ^{18}F-BF-168 (3.9 %ID/g at 2 min after injection; 1.3 %ID/g at 60 min after injection).

Intravenous Administration of BF-227 in Transgenic Mice

In vivo binding of nonlabeled BF-227 to Aβ deposits was examined using PS1/APPsw double transgenic mice. After intravenous injection of 4 mg/kg BF-227, ex vivo observation of transgenic mouse brain slices showed numerous fluorescent spots in the neocortex and hippocampus (Figs. 3A and 3B). In contrast, no fluorescent spots were detected in the wild-type mouse brain (Fig. 3C). Brain sections of transgenic mice were subsequently immunostained using Aβ-specific antibody, and the distribution of plaques labeled with BF-227 corresponded well with Aβ immunostaining (Fig. 3D, arrowheads).

Time–Activity Data of ^{11}C-BF-227 in Clinical PET Study

No toxic event was observed in the current clinical trial of ^{11}C-BF-227. The SUV time–activity curves from ^{11}C-BF-227 PET in AD patients and all normal subjects are shown in Figure 4. Both groups showed rapid entry of ^{11}C-BF-227 into gray matter areas. In AD patients, the frontal, temporal, and parietal cortices, areas known to contain high concentrations of fibrillar amyloid plaques in AD, retained ^{11}C-BF-227 to a greater extent during the later time points compared with normal subjects (Figs. 4A–4C). When the 2 groups were compared, a significant difference in time–activity curves was observed in the frontal (Fig. 4A), lateral temporal (Fig. 4B), parietal (Fig. 4C), and visual association cortices (data not shown). In contrast, time–activity curves in the cerebellum (Fig. 4D), an area lacking fibrillar amyloid plaques, were nearly identical in normal subjects and AD patients. The subcortical white matter region showed relatively lower entry and slower clearance than gray matter areas but no significant difference in time–activity curves between the 2 groups (data not shown). In the comparison of time–activity curves in the cortical areas and cerebellum, AD patients showed a significant difference in time–activity curves over 10 min after administration of ^{11}C-BF-227, but normal subjects showed no significant differences.

SUV Images in AD Patients and Normal Control Subjects

SUV images summed over 20–40 min after injection of an aged normal subject (70-y-old woman) and an AD patient (68-y-old woman; MMSE score = 21) are shown in Figure 5. Cortical retention of ^{11}C-BF-227, especially in the basal portion of the frontal, temporal, and parietal region, was evident in the AD patient, in contrast with the images of the aged normal subject. This pattern of distribution is consistent with the findings of neuritic plaque distribution in postmortem AD brains (*18*). Higher retention of ^{11}C-BF-227 was also observed in the brainstem and thalamus; however, similar retention in these areas was detected in the aged normal subject. ^{11}C-BF-227 uptake in the cerebellum was relatively sparse in both the aged normal subject and the AD patient.

Comparisons of Regional SUVs and SUV Ratios

In the quantitative comparison of regional SUVs between 40 and 60 min after administration, cortical regions showed the tendency to be increased in AD patients; however, the difference was not significant because of the large individual difference in SUVs. SUVs in the thalamus, pons, and white matter were similar in the 3 groups. Because there were no plaques in the cerebellum, there was no BF-227 binding and no significant difference in the SUV between AD and normal groups, indicating that the cerebellum is adequate as a reference region. Therefore, the ratio of regional SUV to cerebellar SUV (SUV ratio) was calculated as an index of ^{11}C-BF-227 retention. This analysis successfully reduced the intersubject variability, as reflected in low SD values (Table 2). The mean SUV ratio for the frontal, lateral temporal, parietal, temporooccipital, occipital, anterior and posterior cingulate cortices, and striatum was significantly greater in AD patients than that in aged normal subjects (Table 2; Fig. 6). Notably, the SUV ratio in the lateral temporal cortex showed no overlap between AD patients and normal control subjects (Fig. 6). The SUV ratio in the medial temporal cortex, thalamus,

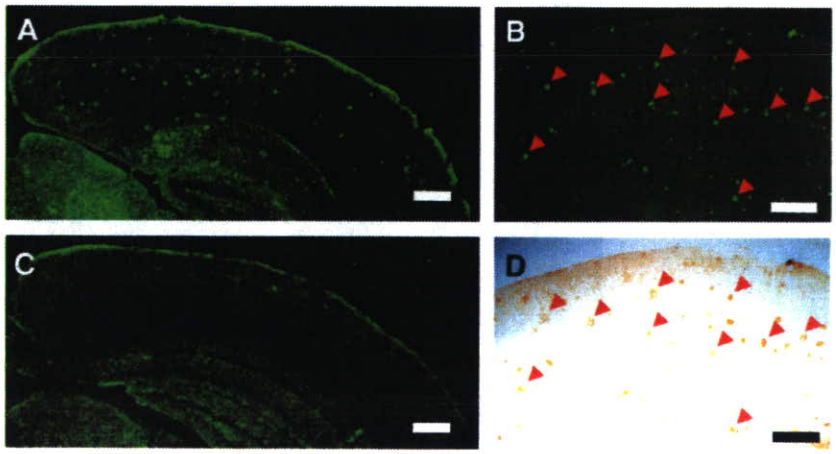

FIGURE 3. In vivo binding of BF-227 to amyloid plaques in PS1/APP transgenic mouse. In brain sections from PS1/APP transgenic mouse after intravenous injection of 4 mg/kg BF-227, numerous fluorescent spots were observed in neocortex and hippocampus of brain (A and B). In contrast, no fluorescent spots were observed in brain of wild-type mouse (C). Distribution of plaques labeled with BF-227 corresponded well with Aβ immunostaining in same section (B and D, arrowheads).

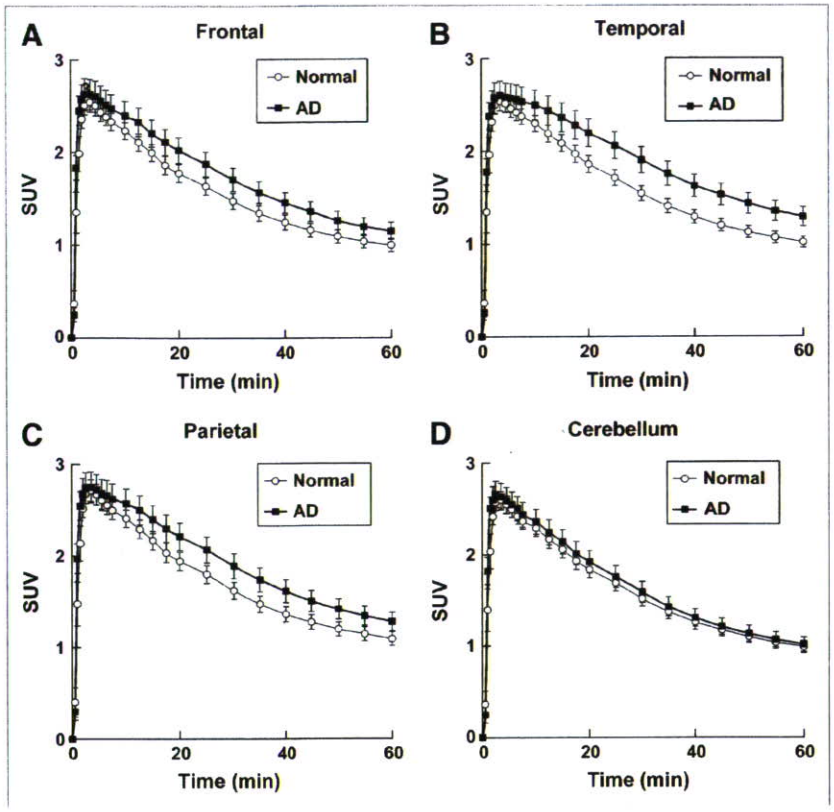

FIGURE 4. Time–activity data for ^{11}C-BF-227 PET in humans. SUV time–activity curves of ^{11}C-BF-227 in frontal cortex (A), temporal cortex (B), parietal cortex (C), and cerebellum (D) are shown. Each point represents mean ± SEM of data from 7 AD patients and 7 normal control subjects.

pons, and white matter was nearly identical in AD patients and normal subjects. The effect size between AD patients and aged normal subjects was highest in the lateral temporal cortex, which was followed by the parietal, anterior cingulate, and frontal cortices, and was lowest in the medial temporal, thalamus, and pons (Table 2). No significant difference was observed in any brain regions between young normal and aged normal subjects, although aged individuals tended to exhibit a higher SUV ratio in the frontal cortex than young individuals (data not shown).

Voxel-by-Voxel Analysis of ^{11}C-BF-227 PET Images

In comparison with aged normal subjects, AD patients showed significantly higher uptake of ^{11}C-BF-227 in the bilateral temporoparietal region ([50, −56, 6], $Z = 5.41$, $k = 22{,}823$), including the posterior cingulate cortex and the left middle frontal gyrus ([−26, 24, 40], $Z = 3.79$, $k = 1{,}401$) in SPM analysis (Fig. 7). These areas corresponded well with the region containing a high density of neuritic plaques. In contrast, no significant region was detected showing lower uptake of ^{11}C-BF-227 in the AD group than that in the normal group.

DISCUSSION

BF-227 was designed to improve BBB penetration and clearance from normal brain tissue, without deteriorating the high binding affinity of benzoxazole derivatives to Aβ. Several lipophilic compounds have been reported as potential amyloid imaging probes. 2-(1-{6-[(2-Fluoroethyl)(methyl)amino]-2-naphthyl}ethylidene)malononitrile (FDDNP) was introduced as the first BBB-permeable compound for in

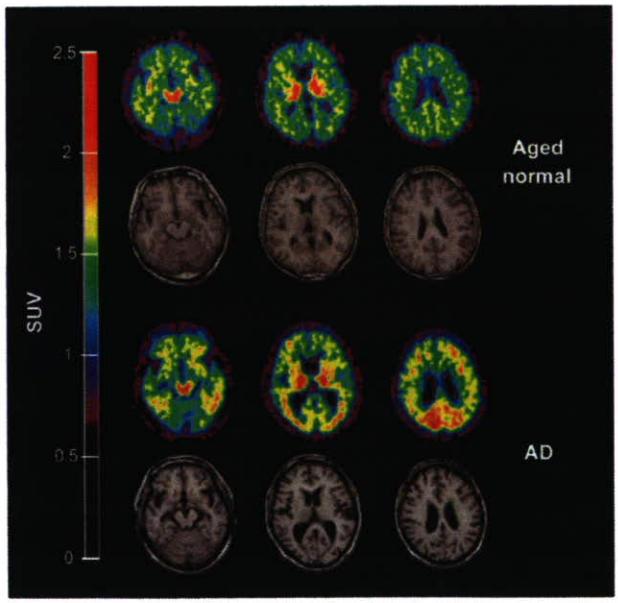

FIGURE 5. Mean SUV images between 20 and 40 min after injection of ^{11}C-BF-227 in aged normal subject (top, 70-y-old woman) and AD patient (bottom, 68-y-old woman). Coregistered MR images are shown below PET images.

TABLE 2
Regional SUV and Regional-to-Cerebellar SUV Ratio of ^{11}C-BF-227 in Normal Subjects and AD Patients

Distribution	SUV			SUV ratio			Cohen's *d*, Aged normal vs. AD
	All normal	Aged normal	AD	All normal	Aged normal	AD	
Frontal	1.13 ± 0.23	1.11 ± 0.24	1.24 ± 0.27	0.99 ± 0.04	0.99 ± 0.05	1.13 ± 0.06*	2.54
Lateral temporal	1.16 ± 0.22	1.15 ± 0.23	1.38 ± 0.30	1.03 ± 0.05	1.02 ± 0.04	1.25 ± 0.06*	4.51
Parietal	1.22 ± 0.24	1.19 ± 0.24	1.36 ± 0.30	1.08 ± 0.06	1.06 ± 0.05	1.24 ± 0.06*	3.26
Temporooccipital	1.22 ± 0.23	1.21 ± 0.24	1.35 ± 0.27	1.08 ± 0.06	1.08 ± 0.06	1.23 ± 0.09*	1.96
Occipital	1.23 ± 0.23	1.21 ± 0.24	1.32 ± 0.26	1.09 ± 0.06	1.08 ± 0.06	1.20 ± 0.07*	1.84
Anterior cingulate	1.19 ± 0.26	1.16 ± 0.26	1.27 ± 0.26	1.04 ± 0.04	1.03 ± 0.04	1.16 ± 0.06*	2.55
Posterior cingulate	1.28 ± 0.25	1.24 ± 0.25	1.38 ± 0.26	1.13 ± 0.08	1.11 ± 0.08	1.26 ± 0.04*	2.37
Medial temporal	1.33 ± 0.24	1.31 ± 0.25	1.31 ± 0.27	1.18 ± 0.07	1.17 ± 0.07	1.20 ± 0.10	0.35
Striatum	1.57 ± 0.34	1.52 ± 0.34	1.62 ± 0.34	1.38 ± 0.08	1.35 ± 0.06	1.47 ± 0.06*	2.00
Thalamus	1.78 ± 0.44	1.70 ± 0.41	1.73 ± 0.36	1.56 ± 0.12	1.51 ± 0.09	1.58 ± 0.11	0.70
Pons	1.90 ± 0.34	1.87 ± 0.34	1.91 ± 0.39	1.68 ± 0.08	1.67 ± 0.08	1.74 ± 0.09	0.82
White matter	1.64 ± 0.27	1.61 ± 0.28	1.69 ± 0.33	1.45 ± 0.11	1.44 ± 0.11	1.55 ± 0.12	0.96
Cerebellum	1.14 ± 0.23	1.13 ± 0.24	1.10 ± 0.23				

*$P < 0.05$ vs. aged normal group.

vivo imaging of amyloid. FDDNP specifically binds to both SPs and NFTs in AD brain sections (*19*). After intravenous injection of FDDNP, greater accumulation was observed in SP- and NFT-rich areas of the human brain (*20*). Thioflavin-T derivatives without any positive charge also show high permeability of the BBB. One of these compounds, PIB, was applied in a human PET study and enabled successful differentiation between AD patients and healthy normal individuals (*5*). Another amyloid-imaging agent, SB-13, was also applied in a human PET study and exhibited binding properties similar to those of PIB (*21*). Several iodinated agents, 6-iodo-2-(4′-dimethylamino-) phenyl-imidazo[1,2-*a*]-pyridine (IMPY) and I-stilbene, have also been explored for use as SPECT probes (*22*). Although validation remains necessary to determine whether retention of these agents in the neocortex truly reflects the level of amyloid deposition, such findings suggest the potential usefulness of this technique for early diagnosis of AD.

The results of the in vitro binding experiment indicate that binding of BF-227 reflects the amount of Aβ fibril deposition. In neuropathologic staining of AD brain sections, the fluorescence intensity of BF-227 is highest in the core region of mature amyloid deposits, which contain dense fibrils of Aβ. Conversely, diffuse plaques containing fewer Aβ fibrils are faintly stained by BF-227. SPs in the cerebellum are predominantly of the nonfibrillar type (*23,24*), and BF-227 only faintly stained diffuse amyloid plaques in the cerebellum. Thus, the absence of ^{11}C-BF-227 accumulation in the cerebellum of AD patients suggests the binding preference of this compound for fibrillar Aβ. This finding also indicates that the cerebellum is suitable as a reference region in the quantitative analysis of ^{11}C-BF-227 PET data.

PIB is currently the most successful of several amyloid-imaging agents. A clinical PET study in AD patients showed higher uptake of PIB in cortical areas and striatum, particularly the frontal and parietal cortices (*5–7*). In contrast, the current study demonstrated higher cortical retention of ^{11}C-BF-227 in the temporoparietal–occipital region rather than that in the frontal cortex and the striatum in AD patients. Both agents are considered to preferentially bind to the β-sheet structure of Aβ fibrils. What other factors could

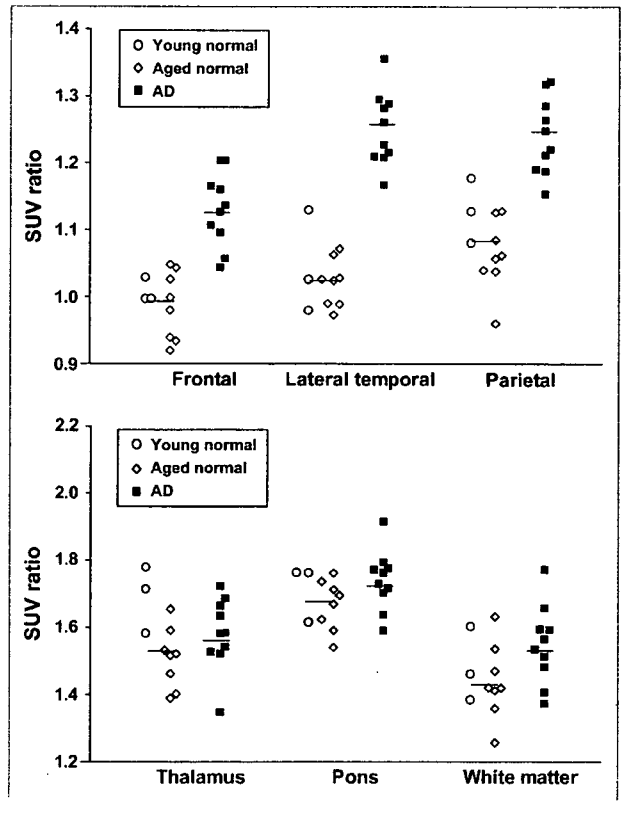

FIGURE 6. ROI/cerebellar SUV ratio in young normal subjects (○), aged normal subjects (◇), and AD patients (■). Vertical bar represents average SUV ratio in all normal subjects ($n = 11$) and AD patients ($n = 10$).

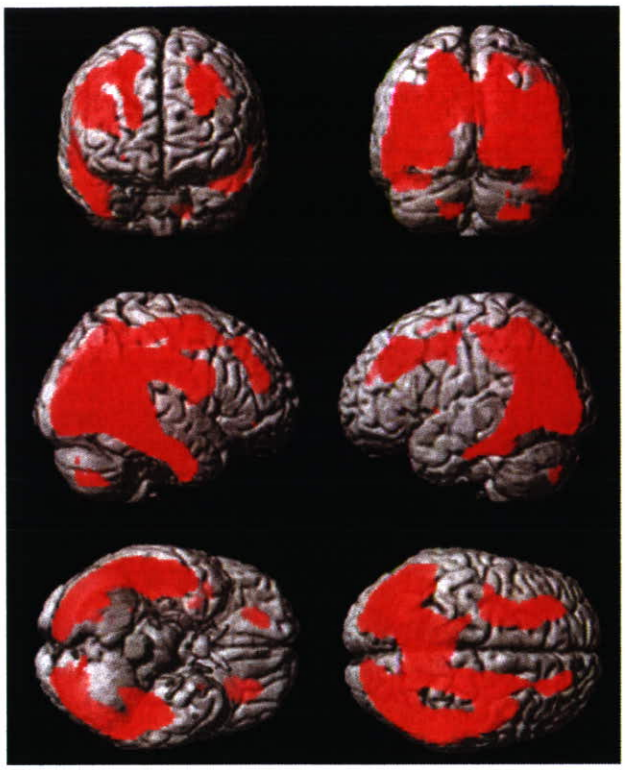

FIGURE 7. Brain regions show significantly elevated SUVs in AD patients compared with data from aged healthy subjects ($P < 0.001$, uncorrected for multiple comparisons).

have caused the difference of tracer distribution between previous PIB studies and the current BF-227 study? Generally, substantial individual variations exist in the amount and spatial distribution of amyloid deposition in AD. Thus, the discrepancy might be partially attributable to a difference in sample populations between studies. To settle this issue, a direct comparison study between PIB and BF-227 should be conducted using the same sample populations. SP is a heterogeneous class of protein aggregates with a β-pleated structure. Compact plaques consist of a dense central core of amyloid fibrils, and noncompact plaques contain less fibrillar Aβ (*25*). Therefore, it would be expected that the lower-affinity compound would tend to detect only SPs with dense Aβ fibrils and that the higher-affinity compound could bind SPs with both dense and moderately fibrillar Aβ. In AD patients, the difference between cortical and cerebellar SUV in ^{11}C-BF-227 PET was less than that in PIB PET (*5–7*), suggesting that the in vivo binding affinity of BF-227 to Aβ deposits is relatively lower than that of PIB. If so, BF-227 binds more preferentially to dense amyloid deposits than PIB. Previous neuropathologic studies have indicated that neuritic plaque densities are highest in the neocortex, especially the temporoparieto–occipital region, and lowest in the cerebellum (*18,26*). Data from SPM analysis are consistent with the postmortem distribution of neuritic plaque deposition in AD patients. Therefore, the difference in cortical distribution between BF-227 and PIB might be due to the difference in binding affinity to Aβ fibrils. A PET probe binding selectively to neuritic plaques would be less subject to Aβ pathology in the normal aging process. Thus, use of ^{11}C-BF-227 PET will allow accurate diagnosis of AD and might reduce false-positive findings in normal individuals. ^{11}C-BF-227 PET might also be useful for tracking the progression of fibrillar Aβ deposition in AD patients. Longitudinal PET investigation of AD patients will elucidate the utility of this imaging technique for monitoring disease progression in AD.

NFTs stained faintly with BF-227, suggesting that BF-227 has a relatively lower binding affinity to NFTs than SPs, which might explain the lack of significant difference in the medial temporal SUV of ^{11}C-BF-227. However, 3 AD patients (AD 1, AD 2, and AD 3 in Table 1) exhibiting high BF-227 accumulation in the cerebral cortex showed higher accumulation in the medial temporal cortex than the other AD patients. This finding might reflect the increasing deposition of amyloid plaques in the medial temporal cortex of the 3 AD patients. Thalamic and white matter accumulation of ^{11}C-BF-227 was considerable in both AD patients and normal subjects. Retention levels of ^{11}C-BF-227 in these regions were nearly identical between normal and AD groups. Therefore, these retentions are not likely to reflect AD-specific pathology. BF-227 retention in these sites may be related to the many myelinated fibers present in these structures, because myelin basic protein—one of the major myelin proteins in the brain—partially shares the same structure with amyloid fibrils, and some β-sheet binding agents bind to this protein (*27–29*). Clearance of ^{11}C-BF-227 from normal brain tissue was slower than that of PIB. This might be caused by the difference in lipophilicity between BF-227 and PIB. BF-227 ($\log P = 1.75$) is more lipophilic than PIB ($\log P = 1.20$) (*30*) because, unlike PIB, BF-227 does not have a hydroxy group. Compounds that are too lipophilic will be bound by plasma protein and undergo rapid metabolism by the liver; therefore, they may display reduced brain uptake. Moreover, lipophilic radioligands display a higher nonspecific binding in the brain and, thus, high nonspecific binding may explain the moderate difference in BF-227 uptake between AD patients and normal control subjects. In general, the introduction of a hydroxy group into a molecule changes the partition coefficient toward more hydrophilicity. Therefore, the hydroxylated BF-227 derivative would be expected to show faster clearance from normal brain tissue and a better signal-to-noise ratio than BF-227. We are now implementing the optimizing process to reduce white matter retention and plan to apply the optimized compound to the candidate for an ^{18}F-labeled PET probe.

CONCLUSION

The present study demonstrated that the benzoxazole derivative BF-227 displays high binding affinity to amyloid

plaques and high BBB permeability. The current clinical trial indicated that BF-227 has adequate safety to be used clinically as a PET probe. ^{11}C-BF-227 PET demonstrated significant retention of this agent in sites with a preference for the deposition of dense amyloid plaques and distinctly differentiated between AD patients and normal individuals. Collectively, these findings suggest that ^{11}C-BF-227 is useful for early diagnosis of AD.

ACKNOWLEDGMENTS

This study was supported by the Program for the Promotion of Fundamental Studies in Health Science by the National Institute of Biomedical Innovation, the Special Coordination Funds for Promoting Science and Technology, the Industrial Technology Research Grant Program in 2004 from the New Energy and Industrial Technology Development Organization of Japan, Health and Labour Sciences Research Grants for Translational Research from the Ministry of Health, Astrazeneca Research Grant 2004, and the Novartis Foundation for Gerontological Research. We appreciate the technical assistance of Dr. Shoichi Watanuki and Dr. Yoichi Ishikawa in the clinical PET studies and Dr. Motohisa Kato in the imaging analysis. We also thank Dr. Hiroyasu Akatsu and Dr. Takayuki Yamamoto for supplying brain samples.

REFERENCES

1. Morris JH, Nagy Z. Alzheimer's disease. In: Esiri MM, Lee VM, Trojanowski JQ, eds. *The Neuropathology of Dementia.* 2nd ed. Cambridge, U.K.: Cambridge University Press; 2004:161–206.
2. Goldman WP, Price JL, Storandt M, et al. Absence of cognitive impairment or decline in preclinical Alzheimer's disease. *Neurology.* 2001;56:361–367.
3. Price JL, Morris JC. Tangles and plaques in nondemented aging and "preclinical" Alzheimer's disease. *Ann Neurol.* 1999;45:358–368.
4. Aisen PS. The development of anti-amyloid therapy for Alzheimer's disease: from secretase modulators to polymerisation inhibitors. *CNS Drugs.* 2005;19:989–996.
5. Klunk WE, Engler H, Nordberg A, et al. Imaging brain amyloid in Alzheimer's disease with Pittsburgh Compound-B. *Ann Neurol.* 2004;55:306–319.
6. Price JC, Klunk WE, Lopresti BJ, et al. Kinetic modeling of amyloid binding in humans using PET imaging and Pittsburgh Compound-B. *J Cereb Blood Flow Metab.* 2005;25:1528–1547.
7. Lopresti BJ, Klunk WE, Mathis CA, et al. Simplified quantification of Pittsburgh Compound B amyloid imaging PET studies: a comparative analysis. *J Nucl Med.* 2005;46:1959–1972.
8. Price JL. Diagnostic criteria for Alzheimer's disease. *Neurobiol Aging.* 1997; 18(suppl):S67–S70.
9. Wang J, Dickson DW, Trojanowski JQ, Lee VM. The levels of soluble versus insoluble brain Aβ distinguish Alzheimer's disease from normal and pathologic aging. *Exp Neurol.* 1999;158:328–337.
10. Okamura N, Suemoto T, Shimadzu H, et al. Styrylbenzoxazole derivatives for in vivo imaging of amyloid plaques in the brain. *J Neurosci.* 2004;24:2535–2541.
11. Okamura N, Suemoto T, Shiomitsu T, et al. A novel imaging probe for in vivo detection of neuritic and diffuse amyloid plaques in the brain. *J Mol Neurosci.* 2004;24:247–255.
12. Shimadzu H, Suemoto T, Suzuki M, et al. Novel probes for imaging amyloid-β: F-18 and C-11 labeling of 2-(4-aminostyryl)benzoxazole derivatives. *J Labelled Compds Radiopharm.* 2004;47:181–190.
13. Jewett DM. A simple synthesis of [^{11}C]methyl triflate. *Appl Radiat Isot.* 1992;43:1383–1385.
14. Iwata R, Pascali C, Bogni A, Miyake Y, Yanai K, Ido T. A simple loop method for the automated preparation of [^{11}C]raclopride from [^{11}C]methyl triflate. *Appl Radiat Isot.* 2001;55:17–22.
15. Holcomb L, Gordon MN, McGowan E, et al. Accelerated Alzheimer-type phenotype in transgenic mice carrying both mutant amyloid precursor protein and presenilin 1 transgenes. *Nat Med.* 1998;4:97–100.
16. Friston KJ, Holmes AP, Worsley KJ, Poline JP, Frith CD, Frackowiack RSJ. Statistical parametric maps in functional imaging: a general linear approach. *Hum Brain Mapp.* 1995;2:189–210.
17. Higuchi M, Tashiro M, Arai H, et al. Glucose hypometabolism and neuropathological correlates in brains of dementia with Lewy bodies. *Exp Neurol.* 2000; 162:247–256.
18. Arnold SE, Hyman BT, Flory J, Damasio AR, Van Hoesen GW. The topographical and neuroanatomical distribution of neurofibrillary tangles and neuritic plaques in the cerebral cortex of patients with Alzheimer's disease. *Cereb Cortex.* 1991;1:103–116.
19. Agdeppa ED, Kepe V, Liu J, et al. Binding characteristics of radiofluorinated 6-dialkylamino-2-naphthylethylidene derivatives as positron emission tomography imaging probes for beta-amyloid plaques in Alzheimer's disease. *J Neurosci.* 2001;21:RC189:1–5.
20. Shoghi-Jadid K, Small GW, Agdeppa ED, et al. Localization of neurofibrillary tangles and beta-amyloid plaques in the brains of living patients with Alzheimer disease. *Am J Geriatr Psychiatry.* 2002;10:24–35.
21. Verhoeff NP, Wilson AA, Takeshita S, et al. In-vivo imaging of Alzheimer disease beta-amyloid with [^{11}C]SB-13 PET. *Am J Geriatr Psychiatry.* 2004;12: 584–595.
22. Kung HF, Kung MP, Zhuang ZP, et al. Iodinated tracers for imaging amyloid plaques in the brain. *Mol Imaging Biol.* 2003;5:418–426.
23. Yamaguchi H, Hirai S, Morimatsu M, Shoji M, Nakazato Y. Diffuse type of senile plaques in the cerebellum of Alzheimer-type dementia demonstrated by beta protein immunostain. *Acta Neuropathol (Berl).* 1989;77:314–319.
24. Yamazaki T, Yamaguchi H, Nakazato Y, Ishiguro K, Kawarabayashi T, Hirai S. Ultrastructural characterization of cerebellar diffuse plaques in Alzheimer's disease. *J Neuropathol Exp Neurol.* 1992;51:281–286.
25. Dickson DW. The pathogenesis of senile plaques. *J Neuropathol Exp Neurol.* 1997;56:321–339.
26. Joachim CL, Morris JH, Selkoe DJ. Diffuse senile plaques occur commonly in the cerebellum in Alzheimer's disease. *Am J Pathol.* 1989;135:309–319.
27. Bjelke B, Seiger A. Morphological distribution of MBP-like immunoreactivity in the brain during development. *Int J Dev Neurosci.* 1989;7:145–164.
28. Ridsdale RA, Beniac DR, Tompkins TA, Moscarello MA, Harauz G. Three-dimensional structure of myelin basic protein. II. Molecular modeling and considerations of predicted structures in multiple sclerosis. *J Biol Chem.* 1997; 272:4269–4275.
29. Stankoff B, Wang Y, Bottlaender M, et al. Imaging of CNS myelin by positron-emission tomography. *Proc Natl Acad Sci U S A.* 2006;103:9304–9309.
30. Mathis CA, Wang Y, Holt DP, Huang GF, Debnath ML, Klunk WE. Synthesis and evaluation of ^{11}C-labeled 6-substituted 2-arylbenzothiazoles as amyloid imaging agents. *J Med Chem.* 2003;46:2740–2754.

Recent Advances in the Development of Amyloid Imaging Agents

Shozo Furumoto[a]*, Nobuyuki Okamura[b], Ren Iwata[c], Kazuhiko Yanai[b], Hiroyuki Arai[d] and Yukitsuka Kudo[a]

[a]*Biomedical Engineering Research Organization, Tohoku University, Sendai 980-8575, Japan,* [b]*Department of Pharmacology, Tohoku University School of Medicine, Sendai 980-8575, Japan,* [c]*Division of Radiopharmaceutical Chemistry, Cyclotron and Radioisotope Center, Tohoku University, Sendai 980-8578, Japan,* [d]*Department of Geriatrics and Gerontology, Tohoku University School of Medicine, Sendai 980-8575, Japan*

Abstract: Excessive amyloid-β (Aβ) deposition in the brain is one of the most crucial events in the early pathological stage of Alzheimer's disease (AD). Therefore, Aβ deposits have enough potential to become a useful biomarker for not only an early diagnosis of AD, but also for the assessment of the clinical efficacy of anti-Aβ therapies, if they can be measured non-invasively and reliably in living patients. As a potent candidate technique to measure this biomarker, PET amyloid imaging using a radioligand for Aβ deposits has received much attention. A large number of Aβ ligands have been synthesized and evaluated as candidates for amyloid imaging agents. These can be classified into six categories of derivatives: Congo-red, Thioflavine T, stilbene, vinylbenzoxazole, DDNP, and miscellaneous. Many of these derivatives exhibit high binding affinities to Aβ fibrils (below 20 nM) and some of them also show excellent brain pharmacokinetic profiles. The concept of amyloid imaging is currently being tested in human PET studies using optimized amyloid imaging agents. Despite the small number of subjects, these studies have demonstrated sufficiently promising results. This review article provides an overview of recent advances in the development of amyloid imaging agents, and includes: a summary of the fundamental basis and clinical significance of amyloid imaging; lists of binding affinity data for 135 compounds classified into 12 molecular frameworks; a comprehensive discussion of the *in vitro* and *in vivo* features of representative Aβ ligands; and a discussion of the current state of clinical evaluation of these amyloid imaging agents (PIB, SB-13, BF-227, and FDDNP).

Keywords: Alzheimer's disease, amyloid imaging, radioligand, PIB, SB-13, BF-227, FDDNP.

1. INTRODUCTION

Alzheimer's disease (AD) is a neurodegenerative disorder clinically characterized by a progressive impairment in cognitive function and behavior, and is the most common form of dementia particularly in elderly [1-4]. It has been estimated that approximately 1% of those aged 60-64 years is affected by AD. The prevalence of AD, however, shows an almost exponential increase with age (doubling approximately every 5 years) after age 60, reaching 20% to 40% of the population over the age 85 [5,6]. The number of patients is predicted to rise in the future due to the expected increase in life expectancy. In terms of social costs, AD is one of the most expensive diseases because it requires not only medication, but also caregiving over a long period [7].

Since the most consistent neurochemical abnormality associated with AD is a severe loss of cholinergic neurons in the areas of the brain related to memory and learning, the current therapeutic approaches are mainly based on the use of acetylcholinesterase inhibitors to preserve brain cholinergic nerve function [8]. This approach can help to prevent some symptoms from becoming worse or to bring modest symptomatic improvements in some patients, but it can not halt the pathological progress of AD. Accordingly, without the advent of appropriate and effective therapies for AD, serious public health problems and the social cost of the disease is expected to increase substantially in the future. That is, there is an enormous medical need for the development of novel therapeutic strategies for AD.

In recent years, great efforts have been made to study the underlying pathogenic mechanisms in AD and translate research advances into the development of new classes of drugs and biomarkers [9-11]. The most widely accepted theory regarding the pathogenic process of AD is the amyloid cascade hypothesis [12-14], which explains that the accumulation and aggregation of amyloid-β (Aβ) peptide in the brain trigger a pathological cascade ultimately leading to neuronal degeneration and dementia. Hence, the major focus of drug development for AD treatment has been directed toward modifying the pathology through lowering the Aβ level in the brain [15-17].

*Address correspondence to this author at Biomedical Engineering Research Organization, Tohoku University, 2-1, Seiryo-cho, Aoba-ku, Sendai 980-8575, Japan; Tel: +81-22-717-7586; Fax: +81-22-717-7586; E-mail: shozo@tubero.tohoku.ac.jp

With the advances in drug development, new biomarkers that can be used for the early diagnosis of AD and clinical evaluation of the disease-modifying drugs targeting Aβ have become increasingly important [18-20]. Based on the amyloid cascade theory, Aβ deposits in the AD brain are probably the most relevant biomarker. Currently, *in vivo* amyloid imaging techniques that can non-invasively and reliably assess Aβ deposition using a tracer that binds to Aβ fibrils have received much attention for their promise in imaging this biomarker [21-25]. A large number of radiotracers have been developed for positron emission tomography (PET) and single-photon emission computed tomography (SPECT) during the past decade [26-29], and some of these have entered into preliminary clinical studies in recent years [29,30].

In this article, we first describe AD pathology, focusing on the amyloid cascade hypothesis, and discuss anti-amyloid therapy for the treatment of AD and the need for biomarkers for AD diagnosis and therapy, leading to a deeper understanding of the fundamental basis and clinical significance of amyloid imaging. We then review amyloid imaging agents, discussing the requirements for tracer development and the compounds that have been reported to date. Finally, we provide an overview of the current state of clinical evaluation of amyloid imaging agents.

2. AD PATHOLOGY AND THE AMYLOID CASCADE HYPOTHESIS

The neuropathological hallmarks of AD are neuritic plaques (NPs) and neurofibrillary tangles (NFTs) in the medial temporal lobe structures and cortical areas of the brain together with selective neuronal and synaptic loss [11,31,32]. NPs, extracellular lesions, consist of a central core of aggregated Aβ peptides [33] surrounded by dystrophic neurites, reactive astrocytes and activated microglia. NFTs represent intracellular bundles of paired helical filaments that are composed of the microtubule-associated protein tau in an abnormally hyperphosphorylated form [34]. Deposition of NPs precedes NFT formation and is relatively specific for AD [13], whereas NFTs are also found in other neurodegenerative disorders [35,36]. While both lesions are indispensable prerequisites for a definitive diagnosis of AD, more attention has focused on the role of Aβ in the pathogenesis of AD. Although the exact mechanisms leading to the development of AD have not been elucidated completely, Aβ is assumed to fulfill a causal role in the pathology of AD (Fig. (1)). This so-called amyloid cascade hypothesis is

1568-0266/07 $50.00+.00

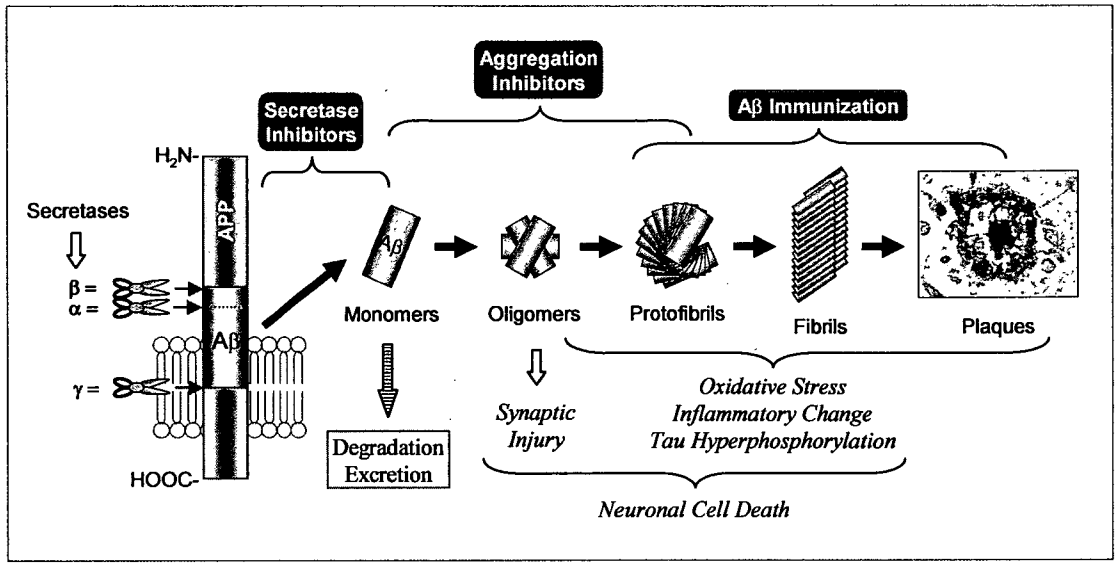

Fig. (1). Schematic illustration of the Aβ amyloid cascade from APP cleavage by secretases to generate Aβ monomers, to plaque formation, via oligomers, protofibrils, and fibrils. Causative factors for neuronal injury are indicated in italic letters under the Aβ pathway. Anti-amyloid agents are also shown in solid-white letters above the therapeutic targets in the Aβ pathway.

widely accepted as the most plausible theory for understanding the pathogenesis of AD.

Aβ is produced from a large membrane-spanning glycoprotein, termed β-Amyloid Precursor Protein (APP) [37], through abnormal sequential cleavages made by proteinases referred to as secretases [38,39]. During the normal processing of APP, namely the non-amyloidogenic pathway, α-secretase first cleaves within the Aβ domain of APP to generate soluble carboxyl-truncated forms of APP, and γ-secretase cleaves the remnant C-terminal proteolytic products further to yield non-amyloidogenic fragments. In the alternative, amyloidogenic pathway, β-secretase instead of α-secretase cleaves APP at the N-terminal site of Aβ, and then γ-secretase cleaves the C-terminal site to release Aβ [40-42]. Although the resulting Aβ peptide varies from 39 to 43 amino acids in length, the main forms of Aβ involved in AD pathology are the shorter 40 amino acid form (Aβ40) and the longer 42 amino acid form (Aβ42). In particular, Aβ42 is the predominant Aβ species found in amyloid plaques in patients with AD, while Aβ40 is the main species of Aβ secreted normally from cells. Aβ42 tends to polymerize and subsequently aggregates more rapidly than Aβ40 [43]; these properties are thought to be associated with both an early onset of AD and an increased risk for AD.

Aβ is produced continuously in the brains of both healthy individuals and AD patients. Under physiological conditions, the Aβ level is tightly controlled by efflux to blood [44] and cerebrospinal fluid (CSF) and proteolytic degradation by amyloid-degrading enzymes, such as insulin-degrading enzyme and neprilysin [45]. The amyloid cascade hypothesis holds that certain pathogenic factors cause an imbalance between the production and clearance of Aβ, leading to a progressive accumulation of Aβ, in particular of Aβ42 peptide [46], in the brain, triggering a cascade of amyloidogenic events as follows. Soluble Aβ excessively accumulated in the brain undergoes a conformational change to acquire a high β-sheet content, stimulating the aggregation of Aβ peptides into soluble oligomers, which have been implicated to impair neuronal and synaptic function by altering membrane permeability [47-49]. These oligomers aggregate further into insoluble fibrils and eventually into immature and amorphous forms of plaques termed diffuse plaques, which are believed to represent the initial phase of plaque formation. These aggregations cause neuronal injury through the induction of oxidative stress [50], inflammatory responses (microglial and astrocytic activation) [51], and abnormal tau hyperphosphorylation, resulting in selective neuronal loss, neurotransmitter deficits, and cognitive symptoms.

The strong evidence for the amyloid cascade hypothesis derives from studies of gene mutations in APP [52] and presenilin-1 and -2 [53], proteins that form the catalytic unit of the γ-secretase protein complex [40]. These various gene mutations all lead to increased levels of Aβ42 and plaque formation in the brain, and all represent a similar clinical entity recognized as an early-onset form of familial Alzheimer's disease (FAD). People with Down's syndrome, who carry an extra copy of the APP gene, also produce higher levels of Aβ from birth, and almost invariably develop amyloid deposits after the age of 30 years [54]. In addition, several studies using transgenic animal models afford convincing supportive evidence for the amyloid cascade theory [55,56]. In one of the most successful models of AD, triple transgenic model mice (3xTg-AD: PS1M146V, APPswe and TauP301L) develop Aβ plaques prior to NFT pathology with a temporal and regional specific profile that closely resembles pathological development in the human brain, including synaptic dysfunction, induction of inflammatory processes, and neurodegeneration [57,58].

Taken together, considerable evidence from a variety of pathological, biochemical, and genetic studies points to Aβ and the process of amyloid deposition, even if not the amyloid deposits themselves, as the upstream causative factor of the pathogenesis of AD.

3. ANTI-AMYLOID THERAPY

According to the amyloid cascade theory, disease-modifying therapy for AD is expected to be performed through lowering the level of Aβ in the brain. Thus, many of the current therapeutic approaches are directed at reducing Aβ accumulation in the brain by modifying different points in the Aβ pathway (amyloid cascade), such as Aβ/APP proteolytic processing, Aβ aggregation, and Aβ clearance.

Because Aβ originates from APP through sequential proteolytic cleavages by β- and γ-secretases, inhibition or modulation of these